6-25-2024

# Quantitative trait loci mapping provides insights into the genetic regulation of dendritic cell numbers in mouse tissues.

Thiago Y Oliveira

Julia Merkenschlager

Thomas Eisenreich

Juliana Bortolatto

Kai-Hui Yao

*See next page for additional authors*

## Authors

Thiago Y Oliveira, Julia Merkenschlager, Thomas Eisenreich, Juliana Bortolatto, Kai-Hui Yao, Daniel M Gatti, Gary Churchill, Michel C Nussenzweig, and Gaëlle Breton

Cell Reports

Article

# Quantitative trait loci mapping provides insights into the genetic regulation of dendritic cell numbers in mouse tissues

## Graphical abstract

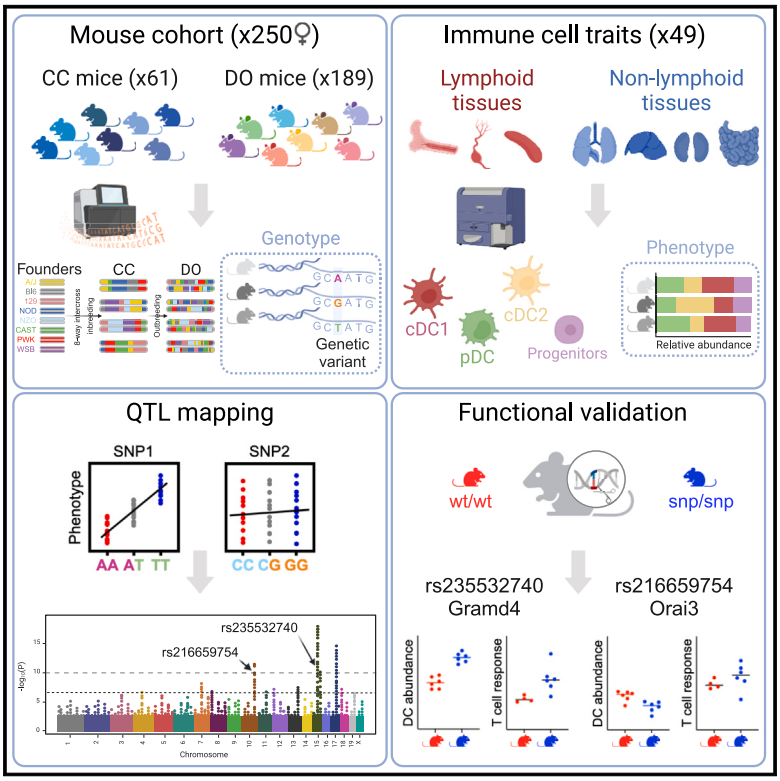


## Highlights

- Collaborative Cross and Diversity Outbred mice show dendritic cell (DC) frequency variation
- QTL mapping reveals the highly polygenic and pleiotropic architecture of DC homeostasis
- Gramd4 and Orai3 regulate DC frequency

## Authors

Thiago Y. Oliveira, Julia Merkenschlager, Thomas Eisenreich, ..., Gary A. Churchill, Michel C. Nussenzweig, Gaëlle Breton

## Correspondence

nussen@rockefeller.edu (M.C.N.), gbreton@rockefeller.edu (G.B.)

## In brief

Oliveira et al. use quantitative trait locus (QTL) mapping in Diversity Outbred mice to find candidate genes linked to dendritic cell (DC) homeostasis. Site-directed mutagenesis using CRISPR-Cas9 confirms two candidate genes, *Gramd4* and *Orai3*. Overall, the data represent a resource for interrogating the mechanisms governing DC homeostasis in tissues.

Oliveira et al., 2024, Cell Reports *43*, 114296
June 25, 2024 
https://doi.org/10.1016/j.celrep.2024.114296

CellPress

Cell Reports

CellPress
OPEN ACCESS

Article

# Quantitative trait loci mapping provides insights into the genetic regulation of dendritic cell numbers in mouse tissues

Thiago Y. Oliveira,[1] Julia Merkenschlager,[1] Thomas Eisenreich,[1] Juliana Bortolatto,[2] Kai-Hui Yao,[1] Daniel M. Gatti,[3] Gary A. Churchill,[3] Michel C. Nussenzweig,[1,4,5,*] and Gaëlle Breton[1,*]

[1]Laboratory of Molecular Immunology, The Rockefeller University, New York, NY 10065, USA
[2]Laboratory of Lymphocyte Dynamics, The Rockefeller University, New York, NY 10065, USA
[3]The Jackson Laboratory, Bar Harbor, ME 04609, USA
[4]Howard Hughes Medical Institute (HHMI), The Rockefeller University, New York, NY 10065, USA
[5]Lead contact
*Correspondence: nussen@rockefeller.edu (M.C.N.), gbreton@rockefeller.edu (G.B.)
https://doi.org/10.1016/j.celrep.2024.114296

## SUMMARY

To explore the influence of genetics on homeostatic regulation of dendritic cell (DC) numbers, we present a screen of DCs and their progenitors in lymphoid and non-lymphoid tissues in Collaborative Cross (CC) and Diversity Outbred (DO) mice. We report 30 and 71 loci with logarithm of the odds (LOD) scores >8.18 and ranging from 6.67 to 8.19, respectively. The analysis reveals the highly polygenic and pleiotropic architecture of this complex trait, including many of the previously identified genetic regulators of DC development and maturation. Two SNPs in genes potentially underlying variation in DC homeostasis, a splice variant in *Gramd4* (rs235532740) and a missense variant in *Orai3* (rs216659754), are confirmed by gene editing using CRISPR-Cas9. *Gramd4* is a central regulator of DC homeostasis that impacts the entire DC lineage, and *Orai3* regulates cDC2 numbers in tissues. Overall, the data reveal a large number of candidate genes regulating DC homeostasis *in vivo*.

## INTRODUCTION

Dendritic cells (DCs) are immune sentinel cells that are found in lymphoid and non-lymphoid organs and are essential for initiating adaptive immune responses and maintaining self-tolerance.[1–5] There are three major classes of DCs that orchestrate immunity. Plasmacytoid dendritic cells (pDCs) produce type I interferon (IFN) in response to viral infections.[6] Conventional dendritic cells (cDCs) are composed of two functionally distinct lineages: CD8α+/CD103+ cDC1 and CD11b+ cDC2. cDC1s are specialized for induction of Th1 $CD4^+$ and $CD8^+$ T cell response,[7–9] whereas cDC2s excel at priming $CD4^+$ T helper cells and promote Th2 and Th17 $CD4^+$ T cell differentiation.[10–14]

All DCs develop from bone marrow (BM) hematopoietic stem cells through a sequence of increasingly restricted progenitors[15–18] (Figure S1A). DC commitment has been associated with a common DC progenitor (CDP),[19–21] which gives rise to pDCs and a cDC precursor (pre-cDC).[22,23] Pre-cDCs subsequently give rise to pre-cDC1 and pre-cDC2, which exit the BM and seed lymphoid and non-lymphoid tissues where they produce fully differentiated cDC1s and cDC2s.[24–27] Within lymphoid tissues, cDC1s and cDC2s can be further divided into lymphoid-resident and tissue-derived populations, the latter representing cells migrating to the lymphoid tissues from the periphery.[1] Notably, pDCs differ from cDCs in that they can develop from both myeloid and lymphoid progenitors, while cDCs are myeloid restricted.[28–30] Nevertheless, pDCs share some phenotypic features of cDCs, including dependence on FMS-related tyrosine kinase 3 ligand and activation-dependent differentiation into cells with a dendritic morphology that can prime naive T cells.

DCs are relatively short-lived,[31–34] and their homeostasis reflects a complex dynamic balance between replenishment from BM progenitor cells,[35] turnover in specialized niches via growth factors,[36–38] and trafficking between non-lymphoid and lymphoid tissues.[39] Maintenance of physiological numbers of DCs is essential as altered DCpoiesis results in abnormal T cell homeostasis,[40,41] and is associated with autoimmune diseases[42–45] and abnormal immune responses.[46–48] Although the precise mechanisms that regulate homeostasis of immune cell numbers including DCs are poorly understood, they are highly heritable, suggesting a strong role for genetics in driving these phenotypic traits.[49–56] Moreover, specific genetic variants related to susceptibility to autoimmune disease have been associated with variation in circulating immune cell frequencies.[57,58] Notably, these findings were limited to peripheral blood cells and did not address the mechanisms controlling development or tissue homeostasis.

Collaborative Cross (CC)[59] and Diversity Outbred (DO)[60] are genetically diverse laboratory mouse populations derived from

a common set of eight inbred founder strains: five laboratory inbred strains (A/J, C57BL/6J, 129, NOD, and NZO) and three wild-derived strains (CAST, PWK, and WSB). CC mice are recombinant inbred strains created by three generations of funnel breeding to integrate genetic contributions from all eight founders, followed by inbreeding to reach near homozygosity.[61] The phenotypes found in CC mice reflect the diversity of immune homeostasis[62,63] and host responses to viral infection.[64–67] The DO mice are outbred animals derived by randomized outbreeding of progenitor CC mice.[60] DO mice show twice the levels of genetic diversity compared to humans and represent a resource for high-resolution genetic mapping. Whereas each CC strain represents a fixed and reproducible genotype, each DO mouse is genetically unique. Together, these genetic resources provide a powerful experimental system to test the hypothesis that variation in DC homeostasis is genetically regulated and to map the source of the diversity.

We performed quantitative trait locus (QTL) analysis using CC and DO mice to map the genetic basis for variation in tissue levels of DCs, finding that the genetic architecture of this complex trait involves multiple loci throughout the genome. To verify the analysis, we narrowed the top QTL regions to likely causal SNPs and verified the effects of two genes, *Gramd4* and *Orai3*, on DC homeostasis by re-creating the non-reference variants in C57Bl/6J mice using CRISPR-Cas9.

## RESULTS

### Variation in DC frequencies in CC and DO mice

We used CC and DO mice to explore the influence of genetics on DC homeostasis. As both sex and non-heritable factors such as age and latent infections can affect variation in immune cell frequencies[51,52,56] and responses,[54,55] we chose to screen co-housed 8- to 10-week-old females to minimize phenotypic variation. We profiled the eight founder strains in triplicate, 61 CC strains and 189 DO mice, for a total of 274 animals (see power simulation in STAR Methods).

Using multiparametric flow cytometry, we conducted a comprehensive screen to enumerate pDCs and cDCs as well as their progenitors in BM, spleen, inguinal lymph node (LN), non-lymphoid tissues (lung, kidney, liver, and intestine) and associated LNs (large intestine LN and small intestine LN) (Figure S1B for gating strategy). pDCs express low levels of MHCII and CD11c and are identified by the expression of BST2. cDCs express high levels of MHCII and CD11c, and the cDC1 and cDC2 mature DCs are defined by reciprocal expression of CD8$\alpha$ and CD11b in lymphoid tissues and of CD103 and CD11b in non-lymphoid tissues. In non-lymphoid tissues, some cDCs lack expression of CD103 and CD11b, and these are referred to as double-negative (DN) cDCs; cDCs that co-express CD103 and CD11b are referred to as double-positive (DP) cDCs. Of note, DP cDCs are the major and more mature cDC2 subset in the small intestinal lamina propria. Although less abundant, DP cDCs are also found in the small intestine associated LNs as well as the lung (Figure S1B). Finally, we used Siglec H and *Ly6C* as lineage markers to distinguish the common and committed DC progenitors in the BM. Altogether we analyzed the frequency of 49 distinct DC subpopulations in 9 different tissues in 274 mice (Table S1, Figures 1A and S2A).

For each phenotype examined, we observed that (1) the frequency of DC subsets in each of the founder strains is reproducible and differs among founders; (2) CC and DO mice exhibited a range of DC subset frequencies similar to those found in founder strains; and (3) DC subset frequencies vary to a greater extent in non-lymphoid tissues (0.01%–15% of CD45$^+$ cells) than in lymphoid tissues (0.01%–2% of CD45$^+$ cells) (Figures 1A, 1B, S2A, and S2B). We next performed Uniform Manifold Approximation and Projection analysis using all 49 phenotypes from CC and DO mice and showed that there is great overall phenotypic diversity across the CC and DO mice (Figure 1C). Although there is diversity among the CC lines regarding the composite of the 49 phenotypes, we do not observe different clusters of mice, but we do have several strains with opposite phenotypes that could be useful for follow-up studies. In summary, CC and DO mice display reproducible variation in DC subset frequencies and represent a useful resource for mapping these phenotypes.

### DC subset composition is tissue specific

DCs are widely distributed in lymphoid and non-lymphoid organs with some notable differences among organs (Figure 2A). Spleen has a significantly higher percentage of cDC2 than cDC1. LNs differ from spleen in that they are dominated by migratory populations and show similar DC subset composition irrespective of anatomic location. In contrast, the composition of DC subsets in non-lymphoid tissues is tissue specific. For example, whereas DP cDCs dominate the migratory population in the small intestine lamina propria, migratory cDC2s dominate in the lung and kidney, and pDCs do so in the liver.

To gain insight into whether there is coordinate DC subset phenotypic variation between or within tissues, we performed Pearson correlation analysis among the 49 traits in 250 CC and DO mice (Figures 2B and 2C). Pairwise comparison of phenotypes showed that cDC subsets are strongly correlated within the 3 LNs tested, lung, liver, kidney, and intestine but not BM and spleen (Figure 2B). Overall, correlations were far weaker across tissues for cDC subsets with the possible exception of inguinal and large intestine LNs as well as intestinal lamina propria and intestine-associated LNs. On the other hand, frequencies of pDCs are correlated between tissues (Figure 2C). The finding that pDC and cDC numbers are differentially regulated is consistent with the hypothesis of their differential origin. However, the number of traits that fail to show a correlation is relatively high. As might be expected, there is no measurable correlation when migratory DC subsets are compared between tissues.

Altogether, our data indicate that DCs display subset- and tissue-specific distribution. In each mouse, the frequency of pDCs in different tissues is correlated. This observation is consistent with the finding that pDCs mature in the BM and enter tissues from the blood. In contrast, the relative distribution of cDCs, whose differentiation takes place in tissues, is correlated within but not between tissues.

### Mapping major QTLs associated with DC homeostasis

To identify QTLs associated with DC homeostasis, we reconstructed the genotype of the CC and DO mice using the mouse

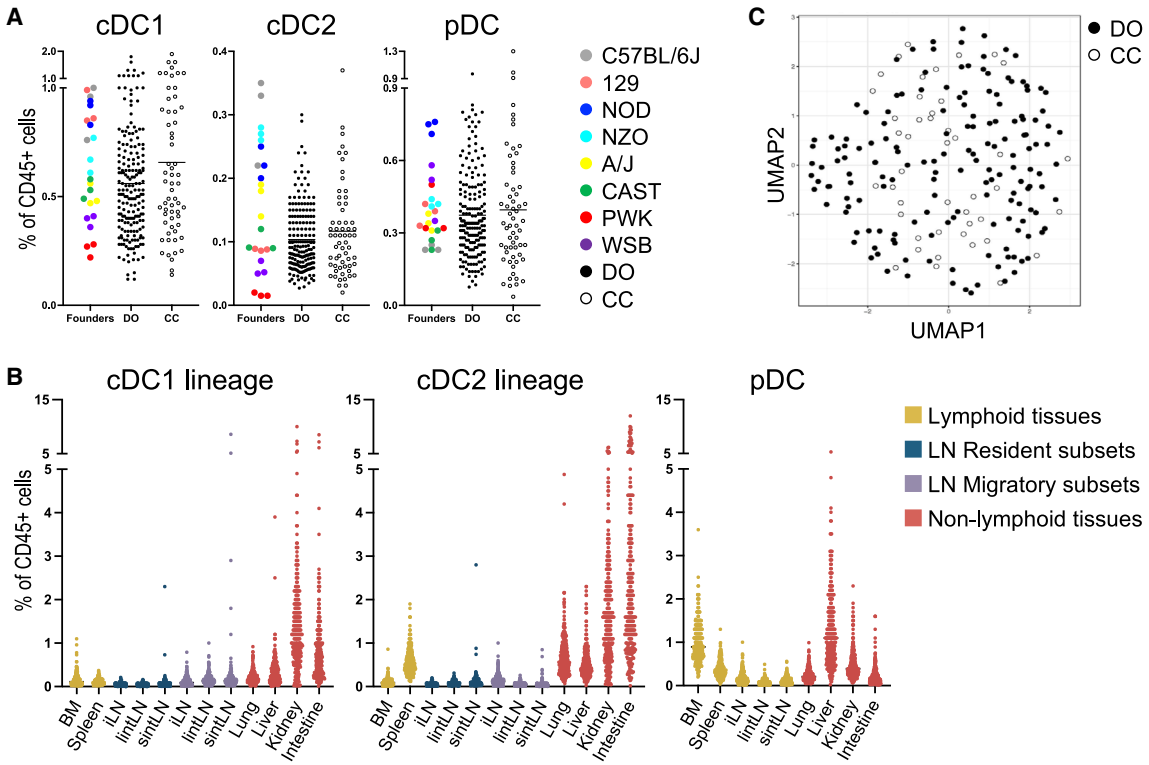


**Figure 1. CC and DO mice show DC frequency variation**

(A) Variation in frequency of spleen cDC1, cDC2, and pDC in C57BL/6J (gray; $n = 3$), 129 (pink; $n = 3$), NOD (blue; $n = 3$), NZO (cyan; $n = 3$), A/J (yellow; $n = 3$), CAST (green; $n = 3$), PWK (red; $n = 3$), WSB (purple; $n = 3$), DO (black; $n = 189$), and CC-RI (open; $n = 61$) mice (see Figure S2A for frequencies of 49 immunophenotypes).

(B) Non-lymphoid tissues show greater DC frequency variation than lymphoid tissues. Comparison of frequency variation along the lineage progression from BM committed progenitor to mature resident and migratory cDC1 and cDC2 as well as pDC across tissues (see Figure S2B for frequencies of 49 immunophenotypes). The gating strategy for DC progenitors and subsets identification in lymphoid and non-lymphoid tissues is shown in Figure S1. Populations included in cDC1 and cDC2 lineages are listed in Table S1.

(C) Uniform Manifold Approximation and Projection (UMAP) analysis using 49 immunophenotypes shows great overall phenotypic diversity across the CC and DO mice.

universal genotyping array (Giga-MUGA).[68,69] We then associated genotype data from the 250 CC and DO mice to the 49 phenotypes using QTL analysis software (R/QTL2).[70] To define the logarithm of the odds (LOD) score threshold for significant QTLs, we used a permutation test, and the 95$^{th}$ percentile of the LOD score distribution is 8.18 (high threshold), the 85$^{th}$ percentile is 7.47, and the 62$^{nd}$ percentile is 6.67 (low threshold).[71] We found 101 QTLs with an LOD score >6.67 spread throughout the genome (Table S2 and Figure 3A). The distribution of QTLs across the 49 phenotypes shows two QTL hotspots on chromosome 15 (Chr15:74,150,521–76,472,763) and chromosome 17 (Chr17:31,340,667–36,781,468) (Figure 3A). Over 60% of QTLs represent phenotypes restricted to lymphoid tissues (BM, spleen, and LNs) with the remaining 40% in non-lymphoid tissues (lung, kidney, liver, and intestine). A minority of QTLs ($n$ = 30) are in the 95$^{th}$ percentile, and these represent phenotypes found in the majority in the lymphoid tissues (Figure 3B). QTLs ($n$ = 20) in the 85$^{th}$ percentile (7.47 < LOD > 8.18) are overrepresented in lung and liver. Finally, most QTLs ($n$ = 51) show LOD scores ranging from 6.67 to 7.47 and represent phenotypes distributed across all tissues (Figure 3B). QTLs were identified in 44 out of 49 traits tested (Figure 3C), each explaining between 5.2% and 22.9% of the phenotypic variation (Table S3). However, the number of cDC2 lineage associated QTLs ($n$ = 30) was greater than cDC1 ($n$ = 23) and pDC ($n$ = 22) lineages (Figure 3D). Notably, QTLs with the highest LOD score are in the cDC2 lineage.

We highlight 3 categories of QTLs (Table 1): *DC markers*. The most significant QTLs were found in chromosomes 1, 7, 15, and 17 in loci that correspond to markers used to identify DCs. We found QTLs with LOD scores >20 associated with DC progenitors (early pre-cDC, pre-cDC, and pre-cDC2) in chromosome 15 (Chr15:74,969,969–75,667,136) driven largely by a WSB mouse strain founder effect. This allele, which contributes uniquely to the observed phenotypic differences, includes 6 private SNPs. The locus contains 38 genes and regulatory regions including *Ly6c*, which is used to identify DC progenitors. A second hotspot is found on chromosome 17 (Chr17:33,938,623–36,781,468) in the MHC locus that encompasses over 250 genes encoding molecules used as lineage markers and others that are implicated in antigen presentation, inflammation, complement system, and innate and adaptive immune responses. This region contains

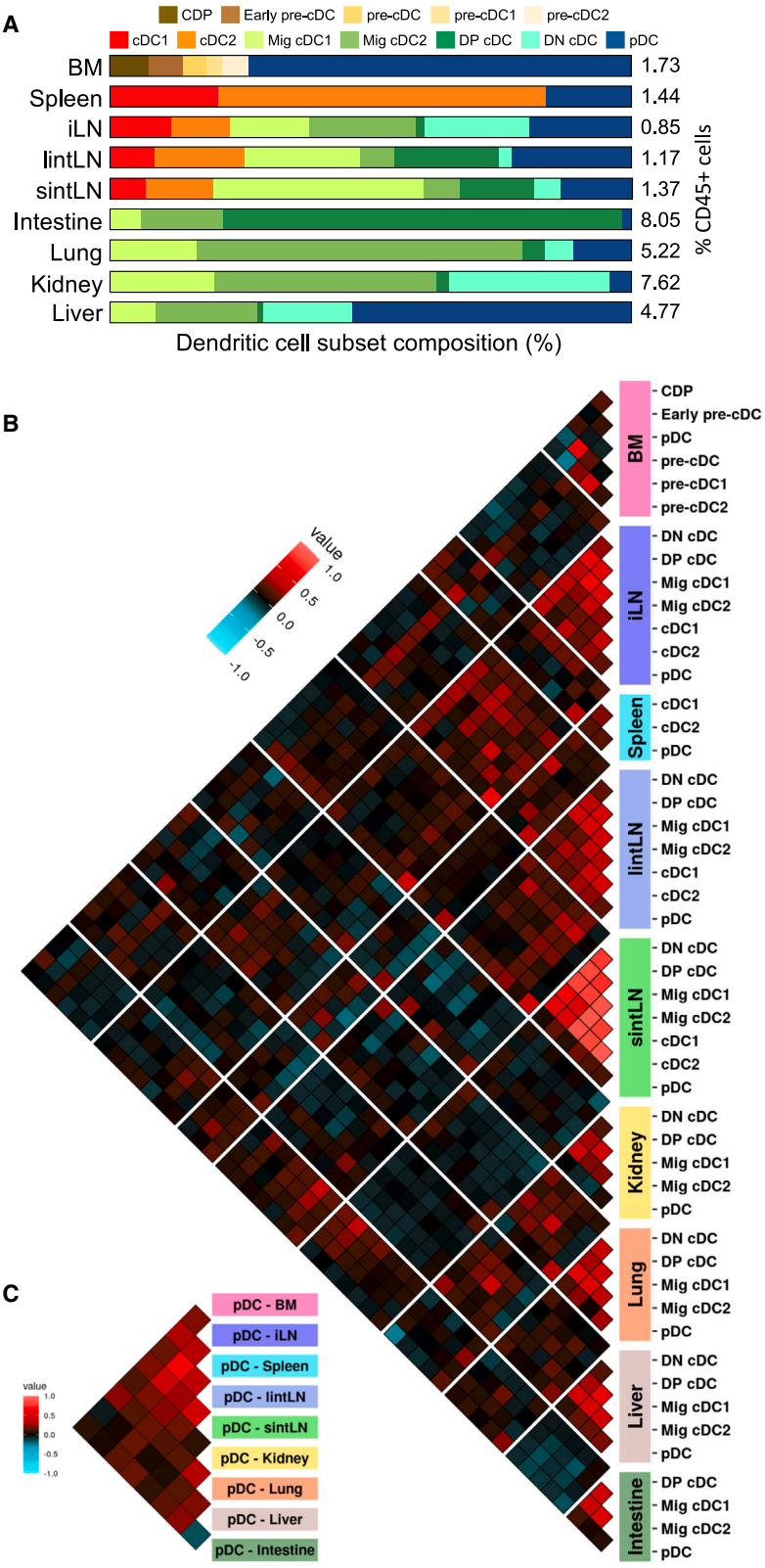


**Figure 2. DC subset composition is largely a function of the tissue site**

(A) Distribution of DC progenitors and subsets across tissues (BM, spleen, inguinal LN, large intestine LN, small intestine LN, intestine, lung, kidney, and liver). Bar graph shows the percentage of the different BM progenitors (CDPs, early pre-cDCs, pre-cDCs, pre-cDC1s, and pre-cDC2s) as well as the composition of cDC1s, cDC2s, Mig cDC1s, Mig cDC2s, DP cDCs, DN cDCs, and pDCs across mouse tissues in the pool of DCs. Data are representative of C57BL/6J mice, with three mice per group. Number on the right is the percentage of total DC progenitors or subsets in $CD45^+$ cells.

(B) Pairwise Pearson correlations among 49 immunophenotypes in CC ($n$ = 61) and DO ($n$ = 189) mice ordered by tissue. Each block represents the correlation between two phenotypes. Correlation is based on between 217 and 250 paired observations, depending on phenotype (see Table S3).

(C) Pairwise Pearson correlations for pDCs (9 immunophenotypes) (extracted from correlation heatmap in B) in CC ($n$ = 61) and DO ($n$ = 189) mice ordered by tissue. Each block represents the correlation between two phenotypes. Correlation is based on between 217 and 250 paired observations, depending on phenotype (see Table S3).

iLN (inguinal LN), lintLN (large intestine LN), sintLN (small intestine LN).

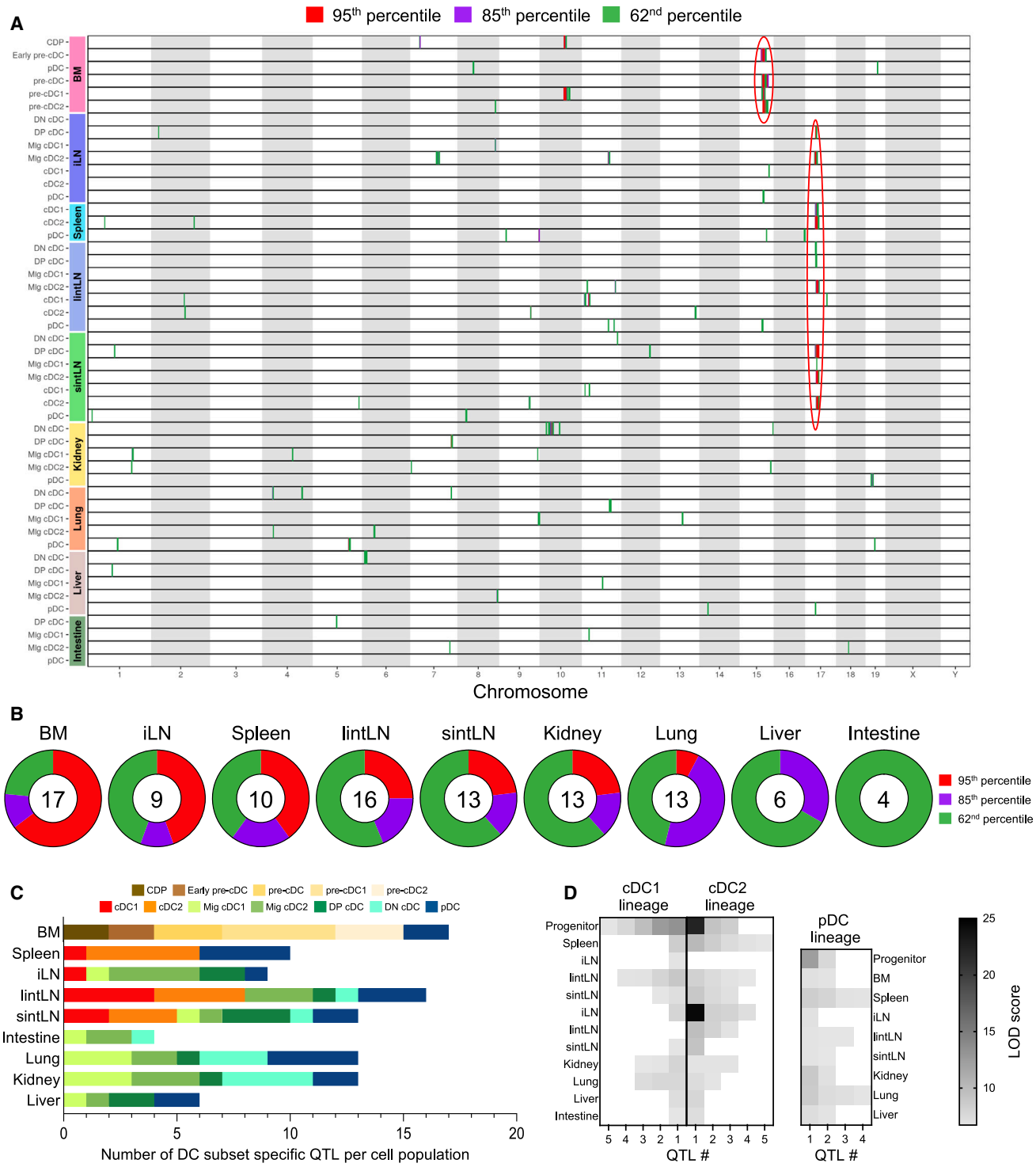


**Figure 3. High-resolution QTL mapping in the CC and DO mice**

(A) QTL map for the 49 traits tested show 101 QTLs with an LOD score >6.67 spread throughout the genome. Each QTL is denoted by a vertical bar; color denotes the QTL distribution in the 95th percentile (red; LOD score >8.19), the 85th percentile (purple; LOD score >7.47), and the 62nd percentile (green; LOD score >6.67).
(B) QTL distribution per tissue (BM, inguinal LN, spleen, large intestine LN, small intestine LN, kidney, lung, liver, and intestine). Red indicates QTLs in the 95th percentile, purple for QTLs in the 85th percentile, and green for QTLs in the 62nd percentile. The number in the inner circle indicates the total number of QTLs for each tissue.
(C) Bar graph shows the number of QTLs for each of the traits tested. QTLs were identified in 44 of the 49 traits tested.
(D) Heatmap showing the number of QTLs per tissue as well as the LOD score for each QTL in the cDC1, cDC2, and pDC lineages. Populations included in cDC1, cDC2, and pDC lineages are listed in Table S1. iLN (inguinal LN), lintLN (large intestine LN), sintLN (small intestine LN).

**Table 1. QTLs associated with DC frequencies**

| | Locus | Phenotype | QTL ID | Chr | QTL position | LOD score | Founder effect |
|---|---|---|---|---|---|---|---|
| DC markers | MHC class II | cDC2_Spleen | 22 | 17 | 36.781468 | 10.27788908 | A/J low |
| | MHC class II | cDC1_Spleen | 23 | 17 | 36.358752 | 8.619977503 | A/J low, WSB low |
| | MHC class II | Mig cDC2_iLN | 31 | 17 | 33.938623 | 24.33795565 | NOD low |
| | MHC class II | Mig DP cDC_iLN | 34 | 17 | 33.949736 | 10.84004278 | NOD low |
| | MHC class II | Mig DP cDC_lintLN | 48 | 17 | 35.01872 | 7.510846783 | CAST low |
| | MHC class II | Mig cDC2_sintLN | 58 | 17 | 35.60663 | 9.426955612 | CAST low, NOD high |
| | MHC class II | Mig DP cDC_sintLN | 61 | 17 | 35.60663 | 9.408758643 | CAST low, NOD high |
| | MHC class II | Mig cDC1_sintLN | 63 | 17 | 35.769078 | 6.803702275 | CAST low |
| | *Ly6c* | pre-cDC2_BM | 2 | 15 | 75.119695 | 22.2144837 | NZO low, WSB high |
| | *Ly6c* | pre-cDC_BM | 9 | 15 | 74.969969 | 23.84560233 | NZO low, WSB high |
| | *Ly6c* | Early pre-cDC_BM | 13 | 15 | 75.342179 | 28.19551147 | WSB low, NZO high |
| | *Cd11b*, *Cd11c* | Mig DP cDC_Kidney | 86 | 7 | 127.953525 | 9.978038674 | CAST high |
| | *Cd45* | Mig cDC1_Kidney | 91 | 1 | 137.405636 | 8.086829096 | CAST low |
| DC homeostasis | *Ccr9*, *Xcr1* | pDC_Spleen | 25 | 9 | 123.261519 | 8.537908996 | Bl6 low, PWK high |
| | *Ccr9*, *Xcr1* | Mig cDC1_Lung | 73 | 9 | 123.971263 | 7.81203802 | Bl6 low, PWK high |
| | *Bcl11a* | cDC1_lintLN | 43 | 11 | 23.752504 | 9.100272325 | PWK high |
| | *Bcl11a* | cDC1_sintLN | 57 | 11 | 23.752504 | 7.294866664 | PWK high |
| | *Cd274* | pDC_Lung | 82 | 19 | 29.719767 | 7.430637435 | PWK low, WSB high |
| | *Ccl1*, *Ccl2*, *Ccl8*, *Ccl11* | pDC_lintLN | 50 | 11 | 82.254855 | 6.723323086 | CAST low |
| | *Flt3* | cDC2_sintLN | – | 5 | 146.899976 | 6.460069909 | PWK low, 129 high |
| | *Il3ra* | pDC_Liver | – | 14 | 14.515357 | 6.134753512 | A/J low, PWK high |
| Shared | – | Mig cDC2_Lung | 70 | 4 | 35.145013 | 6.85751712 | A/J low, Bl6 high |
| | – | Mig DN cDC_Lung | 76 | 4 | 35.021101 | 7.952831089 | A/J low, Bl6 high |
| | – | pre-cDC1_BM | 4 | 10 | 77.848471 | 12.58358558 | Bl6 low, PWK high |
| | – | CDP_BM | 15 | 10 | 77.563 | 12.38904864 | PWK low, Bl6 high |
| 95th percentile | – | Early pre-cDC_BM | 12 | 15 | 68.448939 | 11.10801649 | WSB low, NOD high |
| | – | pre-cDC_BM | 11 | 15 | 86.581607 | 10.66832022 | NZO low, A/J high |
| | – | pre-cDC1_BM | 5 | 10 | 79.874293 | 13.31382668 | 129 low, PWK high |
| | – | pre-cDC1_BM | 8 | 15 | 76.472763 | 9.809605981 | A/J low, NZO high |
| | – | pre-cDC2_BM | 3 | 15 | 82.404619 | 9.451212195 | NZO low, A/J high |
| | – | pre-cDC2_BM | 1 | 8 | 117.482563 | 8.55622007 | WSB high |
| | – | cDC1_lintLN | 42 | 11 | 10.06037 | 8.108979485 | NZO low, WSB high |
| | – | cDC2_Spleen | 21 | 17 | 32.441452 | 8.704368631 | A/J low, Bl6 high |
| | – | cDC2_sintLN | 55 | 17 | 40.955272 | 9.029027256 | A/J low, NOD high |
| | – | cDC2_lintLN | 38 | 9 | 97.290387 | 8.31650588 | CAST low, 129 high |
| | – | Mig cDC1_iLN | 32 | 8 | 117.47005 | 8.002861176 | NOD low, PWK high |
| | – | Mig cDC2_lintLN | 47 | 17 | 41.317433 | 9.826735683 | CAST low, Bl6 high |
| | – | Mig cDC2_iLN | 30 | 11 | 84.790727 | 8.408946183 | NOD low, Bl6 high |
| | – | Mig cDC2_lintLN | 46 | 11 | 103.728036 | 8.278415807 | NOD low, Bl6 high |
| | – | Mig cDC2_iLN | 29 | 7 | 89.15195 | 8.229291384 | NOD low, Bl6 high |
| | – | Mig DN cDC_Kidney | 88 | 10 | 40.165239 | 9.486641375 | CAST low, PWK high |
| | – | pDC_Spleen | 27 | 16 | 96.332995 | 8.056688725 | NZO low, CAST high |
| | – | pDC_Kidney | 95 | 19 | 23.843845 | 8.959664076 | CAST low, WSB high |
| | – | pDC_Lung | 80 | 5 | 112.830419 | 8.847002318 | 129 low, Bl6 high |

QTLs with LOD scores ranging from 6.5 to 24.3 associated with the number of spleen cDCs and migratory cDCs in LNs. However, the founder effects for these QTLs differed between spleen and LNs, with A/J being a significant driver in spleen, NOD in inguinal LN, and CAST in the intestine LNs. Thus, these traits appear to be governed by distinct tissue-specific genetic elements. Two other QTLs with LOD scores of 8 and 10 were found on chromosomes 1 (Chr1:137,405,636–137,638,703) and 7 (Chr7:127,953,525),

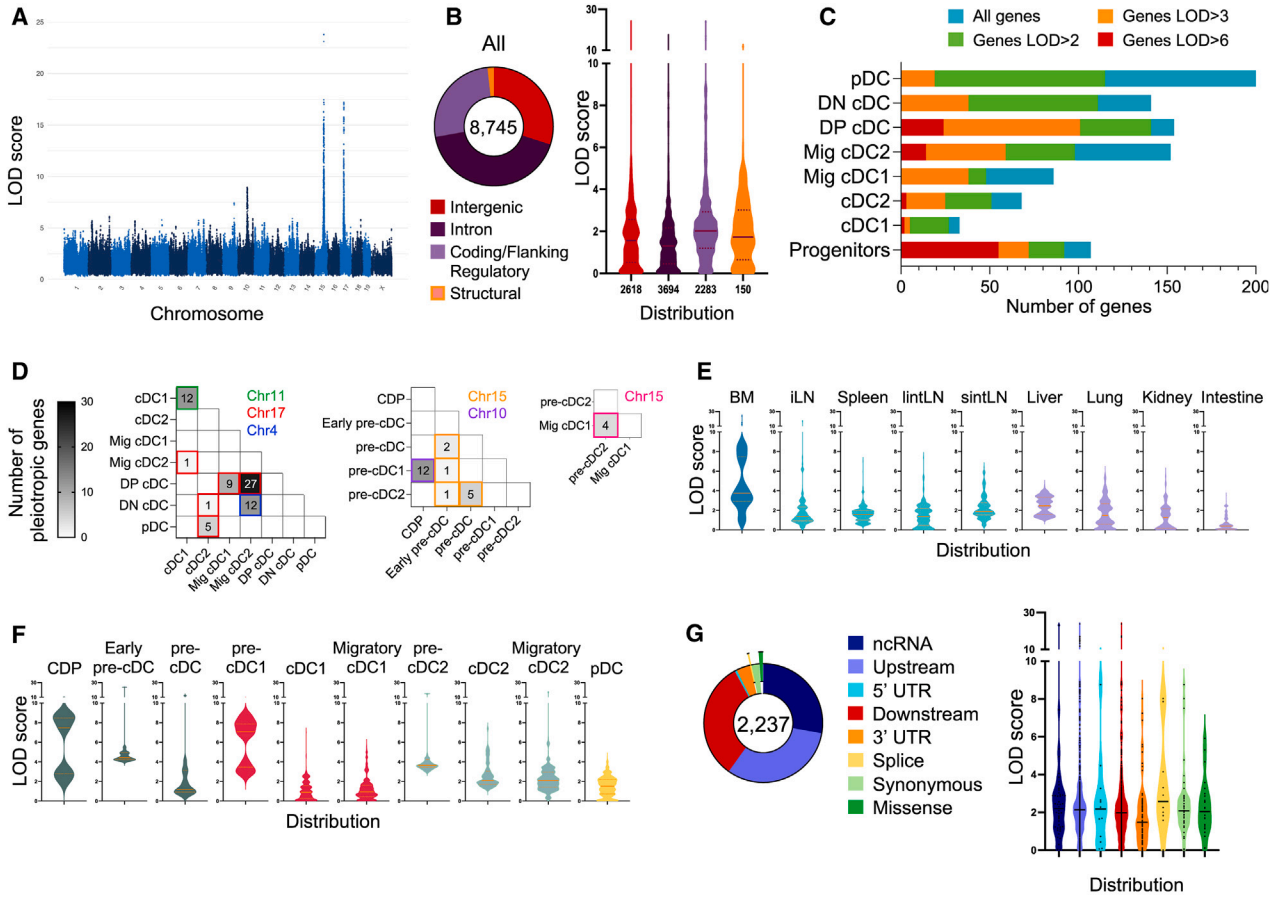


*(legend on next page)*

respectively, in the *Cd45* and *Cd11c/Cd11b* loci that encode lineage-associated markers. The CAST genotype is a significant driver of these QTLs, and it contains 47 SNPs, all private variants in 25 genes for Chr7, and 119 SNPs with 47 private variants mainly in regulatory elements and in 4 genes for Chr 1.

### Genes with defined roles in DC homeostasis

QTLs with an LOD score of ~8 associated with pDCs and migratory cDC1 were found on chromosome 9 (Chr9:123,261,519–123,971,263) in a region that encompasses *Ccr9* and *Xcr1*. CCR9 is used as a marker for a subset of pDCs and controls their migration.[72,73] XCR1 is a chemokine receptor expressed by resident and migratory cDC1, which also serves as a lineage marker for cross-presenting DCs.[7,8] PWK contributes to the founder effect to this multi-trait locus that contain 269 SNPs, with 11 SNPs in *Ccr9* and 2 in *Xcr1*, all in regulatory regions. QTLs with LOD scores of 7 and 9 associated with cDC1 in LNs were found on chromosome 11 (Chr11:23,752,504) in a region that includes the *Bcl11a*, an essential lineage-specific transcriptional repressor.[74] Four additional QTLs with LOD scores ranging from 6.1 to 7.4 associated with cDC2 and pDCs were found in the region of *Il3ra*, *Flt3*, *Cd274*, *Ccl1*, *Ccl2*, *Ccl8*, and *Ccl11*, all of which have been implicated in DC development or trafficking.[6,35–37,75–79]

### QTLs associated with two or more DC subpopulations

QTLs shared by two or more DC subpopulations could have pleiotropic effects. These QTLs have the same founder effect and associated SNPs. Two QTLs with LOD scores ranging from 6.85 to 12.6 associated with multiple DC subpopulations were found on chromosome 4 (Chr4:35,145,013) and chromosome 10 (Chr10:77,563). Genes found in these regions include *Itgb2*, *Slc35a1*, *Cga*, *Zfp292*, and *Orc3*.

In conclusion, QTL mapping using CC and DO mice revealed both known regulators of DC development and migration and genetic intervals that appear to contribute to DC homeostasis.

## Genetic architecture of a complex trait

We investigated SNPs associated with 101 QTLs with LOD scores >6.67 (Table S2) to try to define causal genes related to specific traits. As shown in a Manhattan plot, the distribution of SNPs across the 49 phenotypes shows that SNPs with the highest LOD score are in chromosomes 15, 17, and 10 (Figure 4A and Table S4). For each QTL, we considered only SNPs that achieve an LOD threshold of 1.5 or less below the top LOD score.[80] Across all 8,745 SNPs that pass the cutoff, we observed a significant enrichment of SNPs with LOD scores <6 and a much smaller number of SNPs with LOD scores ranging from 6 to 23.8 (96.9% vs. 3.1% respectively). Causal SNPs include non-coding (i.e., intergenic and intron variants; 72.6%), coding/flanking/regulatory (25.8%), and far less frequent structural variants (1.6%) (Figure 4B). We found 856 genes associated with the 101 QTLs, which reveal the polygenic architecture of DC homeostasis. However, we found only 98 genes (10.4%) with a high LOD score (LOD > 6), which are distributed between progenitors, cDC1, cDC2, Mig cDC2, and DP cDC (Figure 4C). Finally, we identified 92 pleiotropic genes with lead SNPs affecting at least two traits. The most pleiotropic locus associated with the largest number of traits is the MHC region (chr17: 33.9–36.8 Mb), containing 43 pleiotropic genes (Figure 4D).

We next examined how causal SNPs are distributed among tissues. The data revealed that SNPs with higher LOD scores were found primarily in lymphoid tissues. In particular, BM stands out as the tissue with the greatest number of SNPs with LOD scores >6 (Figure 4E). Liver, lung, kidney, and intestine are enriched in SNPs with LOD scores <6. Notably, lymphoid tissues, i.e., BM, iLN, and spleen, have a relatively lower number of causal SNPs ($n$ = 2,098) than non-lymphoid tissues and the intestine associated LNs ($n$ = 6,647) (Figure S3A). However, there was no major difference in the distribution of the type of genetic variants found in different tissues (Figure S3A).

To determine whether causal SNPs are differentially distributed among DC subpopulations, we examined each independently. The cDC1 and cDC2 lineages differ in that the cDC1 lineage has a greater number of associated causal SNPs with higher LOD scores (6–10), most of them at the pre-cDC1 stage. For the cDC2 lineage, the SNPs with higher LOD score (6–24) are distributed between the pre-cDC2, cDC2, and Mig cDC2 subpopulations. pDCs show a large number of causal SNPs with relatively low LOD scores (Figure 4F). Finally, we did not observe a major difference in the distribution of the type of genetic variants

**Figure 4. Genetic architecture of DC homeostasis complex trait**

(A) Manhattan plot showing all mouse annotated SNPs. For each SNP, the best $p$ value observed among all assessed traits is plotted on a –log10 scale (y axis), according to its genomic coordinates (x axis).

(B) Pie chart show the proportion of associated SNPs identified in 44 phenotypes that map in intergenic (red), intron (purple), or coding/flanking/regulatory (lilac) regions as well as structural variants (orange). The number in the inner circle indicates the total number of associated SNPs. Violin plots show the LOD score distribution of SNPs in intergenic ($n$ = 2,618), intron ($n$ = 3,694), coding/flanking/regulatory ($n$ = 2,283) regions, and structural variants ($n$ = 150).

(C) Bar graph showing the number of SNP-associated genes for each cell type: all genes (blue), genes with LOD >6 (red), genes with LOD >3 (orange), and genes with LOD >2 (green).

(D) Heatmap showing trait-associated gene pleiotropy. Shading indicates the number of pleiotropic genes shared by two cell subsets. Colors depict the pleiotropic loci.

(E) Violin plots showing the LOD score distribution of associated SNPs across tissues.

(F) Violin plots showing the LOD score distribution of associated SNPs across cell type.

(G) Distribution of coding/flanking regions and regulatory element variants identified in 44 phenotypes: ncRNA (blue), upstream (purple), 5′ UTR (cyan), downstream (red), 3′ UTR (orange), splice (yellow), synonymous (light green), and missense (green) variants. The violin plot shows LOD score distribution, and pie chart shows repartition. The number in the inner circle indicates the total number of associated SNPs.

(H) Circos plot showing selected candidate genes. To narrow the search for candidate genes, we focused on coding/flanking variants that have an LOD score >2.5. Colors indicate the type of SNP variant: upstream (purple), downstream (red), 5′ UTR (cyan), 3′ UTR (orange), splice (yellow), and missense (green) variants. If a gene contains multiple SNPs, the type of SNP is displayed as a colored circle. See a list of selected candidate genes in Table S5. Importantly, DP cDCs are the major and more mature cDC2 subset in the small intestinal lamina propria; therefore, we included Mig DP cDCs and not Mig cDC2s in the analysis in Figures 4F and 4H (see Table S1). iLN (inguinal LN), lintLN (large intestine LN), sintLN (small intestine LN).

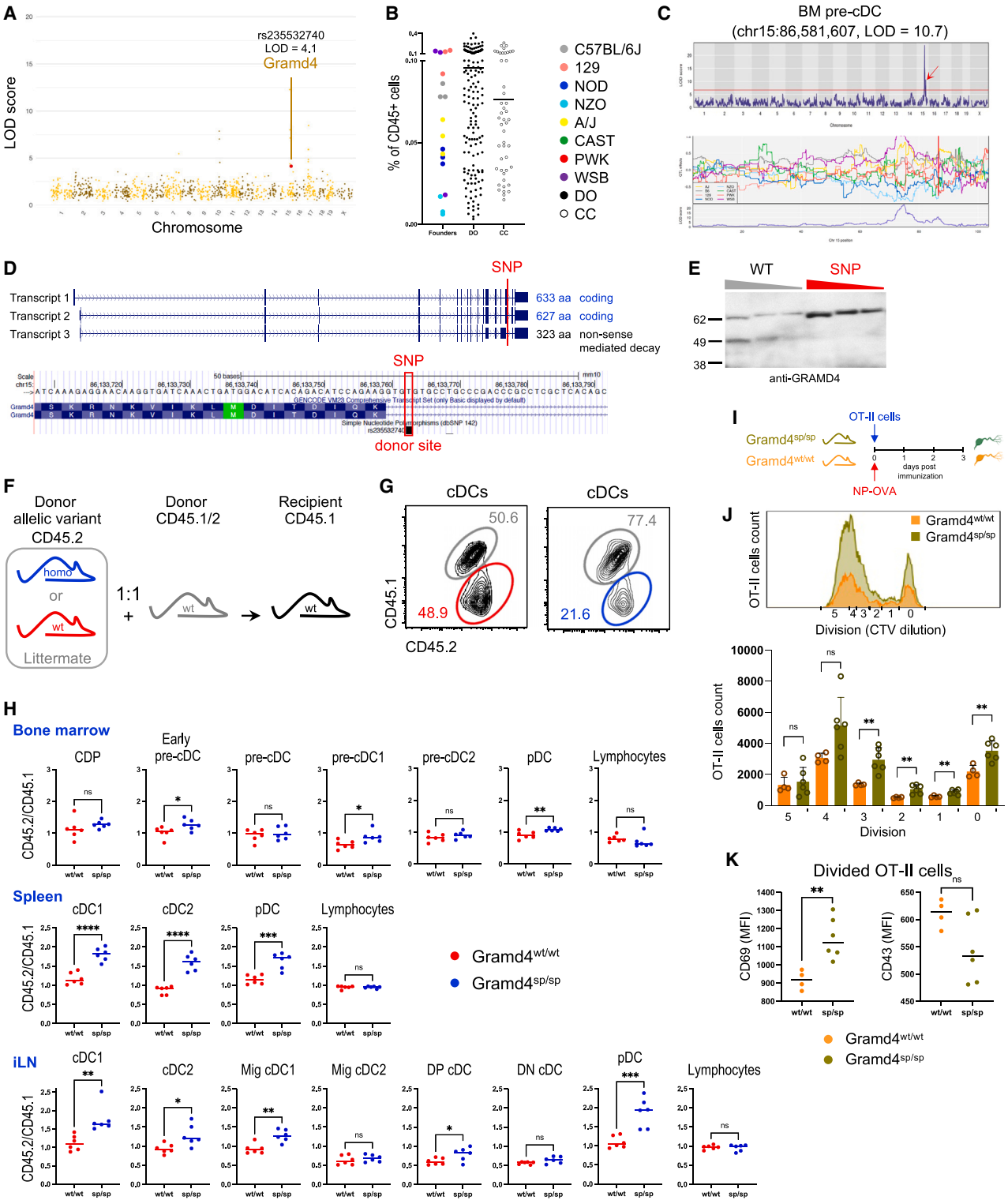


**Figure 5. A QTL in chromosome 15 reveals *Gramd4* as a central regulator of DC homeostasis**

(A) Manhattan plot showing all splice variant SNPs across the 49 phenotypes. For each splice variant, the best *p* value observed among all assessed traits is plotted on a –log10 scale (y axis), according to its genomic coordinates (x axis). *Gramd4* splice variant chosen for validation is highlighted in red.

(B) Variation in frequency of BM pre-cDCs in C57BL/6J (gray; $n = 3$), 129 (pink; $n = 3$), NOD (blue; $n = 3$), NZO (cyan; $n = 3$), A/J (yellow; $n = 3$), WSB (purple; $n = 3$), DO (black; $n = 170$), and CC-RI (open; $n = 47$) mice.

*(legend continued on next page)*

across cell type, with the exception of the early pre-cDC that is dominated by intergenic SNPs (Figure S3B).

Altogether, DC homeostasis is a complex trait with a highly polygenic and pleiotropic architecture. Moreover, SNPs associated with DC specification in lymphoid tissues have high LOD scores, whereas SNPs associated with non-lymphoid tissue phenotypes that show greater variation have lower LOD scores.

## Identification of candidate genes underlying DC homeostasis traits

A large proportion of causal SNPs map to a noncoding part of the genome, and therefore, understanding their relationship with phenotype is challenging. To narrow the search for genes that impact DC homeostasis, we focused on 2,237 variants in coding and flanking regions, as well as regulatory elements (Figure 4G and Table S4). Of note, there is no major difference in the distribution of this type of SNP across DC subsets (Figure S3C). We limited our search to genetic variants with strong founder allele effect underlying the associated QTL. In addition, SNPs in genes with a defined function and appropriate tissue and cellular expression were prioritized. Applying these criteria reduced the causal variants to 104 genes distributed among the 44 subpopulations of DCs studied (Table S5 and Figure 4H). As might be expected, we observed a strong enrichment for enhancer and promoter variants, suggesting that many causal variants may affect gene expression. Apart from the genes with a defined role in DC homeostasis (*Bcl11a*, *Cd274*, *Flt3*, *Ccr9*, *Ccl1*, *Ccl2*, *Ccl8*, *Ccl11*, *Xcr1*, and *Il3ra*), we identified transcription factors (*Zfat*, *Zfp811*, *Zfp292*, *Zfp563*, *Zfp871*, *Zfp592*, *Zfp458*, *Zfp85*, *Zfp874a*, *Zfp58*, *Zfp493*, *Zfp748*, and *Zfp871*), genes involved in metabolism (*Orai3*, *Hps4*, *Orc3*, *Inpp5b*, *Coro1a*, *Abca8a*, and *Abca7*), solute carrier transporters (*Slc35a1*, *Slc22a16*, *Slc35a1*, *Slc28a1*, *Slc6a20a*, and *Slc6a20b*), cell differentiation (*Fes*, *Lst1*, and *Cchcr1*), signaling (*Dgat1*, *Pou5f1*, *Pde4d*, *Plcg2*, *Tyk2*, and *Cdc37*), transcription (Brd2 and Brd4), apoptosis (*Zdhhc3*, *Sulf1*, *Atp2a1*, *Nupr1*, *Aldoa*, *Sult1a1*, and *Gramd4*), chemokine receptor (*Ccr1*), cilium movement (*Mks1* and *Dnah12*), splicing (*Tfip11*), and cytokine/inflammation (*Ltb* and *Tnf*).

## Validation

To validate the approach, we selected two coding variants, a splice variant in *Gramd4* (rs235532740, LOD = 4.1) (Figure 5A) and a missense variant in *Orai3* (rs216659754, LOD = 4.7) (Figure 6A), for further analysis using CRISPR-Cas9 to edit the genome of C57BL/6J mice.

*Gramd4* is found within a QTL in chromosome 15 (Chr15:86,581,607, LOD = 10.7) that is associated with pre-cDC development in the BM (Figure 5B) and also linked to a second neighboring QTL (Chr15:74,969,969, LOD = 23.8) (Figure 5C). The same founder haplotypes contribute to the phenotypic differences in the 2 QTLs and recapitulate the phenotype seen in founders (Figures 5B and 5C). Among the 26 SNPs mapping to this QTL, 8 were in *Gramd4*, and one of these was a splice variant present in four founders, i.e., 129, NZO, CAST, and PWK (Table S4). Although *Gramd4* function has not been studied in immune cells including DCs, it has been implicated in regulation of apoptosis.[81] We used CRISPR-Cas9 to introduce the relevant splice site mutation into the genome of C57BL/6J mice (*Gramd4*$^{sp/sp}$) (Figure 5D). Homozygous *Gramd4*$^{sp/sp}$ mice were born at normal mendelian frequencies. Introduction of the splice variant in *Gramd4*$^{sp/sp}$ mice abrogates splicing (Figure 5E). To determine whether the *Gramd4*$^{sp/sp}$ variant produces an advantage in DC development, we created 50:50 *Gramd4*$^{sp/sp}$:*Gramd4*$^{w/w}$ BM chimeric mice using CD45.1 or .2 to identify the two donors (Figures 5F and 5G). Lymphocytes were present at approximately the expected 50:50 ratio in all tissues tested. As shown in Figure 5H, we analyzed the DC lineage-specific chimerism and showed an increase in DC progenitor and subset frequencies bearing the SNP in all lymphoid tissues, except for the migratory cDC2s. Finally, to determine whether these differences in DC frequencies could impact T cell responses, we adoptively transferred OT-II cells into *Gramd4*$^{sp/sp}$ and *Gramd4*$^{w/w}$ mice and immunized the mice with 4-hydroxy-3-nitrophenylacetyl hapten conjugated to an OT-II ligand peptide OVA$^{328–339}$ [82] (Figure 5I). *Gramd4*$^{sp/sp}$ mice showed a significant increase in the recruitment and proliferation of OT-II cells in draining LN when compared to *Gramd4*$^{w/w}$ mice (Figure 5J). Moreover, divided OT-II cells from *Gramd4*$^{sp/sp}$ mice have a higher level of CD69 and less CD43 than OT-II cells from *Gramd4*$^{w/w}$ mice (Figure 5K), indicating an enhanced activation phenotype and a greater capacity to proliferate. In summary, *Gramd4* is a central regulator of DC homeostasis whose effect is seen in early DC progenitors as well as differentiated DCs.

(C) A QTL driving the frequency of BM pre-cDCs found within chromosome 15 (chr15:86,581,607, LOD = 10.7) that appears to be driven by an A/J and NZO founder effect.
(D) *Gramd4* gene structure and schematic representation of alternative splicing (UCSC Genome Browser). SNP localization is shown in red.
(E) Western blot on total splenocytes from *Gramd4*$^{w/w}$ and *Gramd4*$^{sp/sp}$ mice showing alternative splicing.
(F) Schematic representation of mixed BM chimera experiment.
(G) Representative flow cytometry plot for mixed BM experiment.
(H) Frequencies of DC progenitors and subsets in mixed BM chimera mice due to differential expression of *Gramd4* SNP variant in BM, spleen, and inguinal LN. Chimerism is expressed as the ratio between the number of CD45.2 and CD45.1/CD45.2 cells for each cell population. Representative of 2 independent experiments; each dot represents one mouse, $n = 6$ per group, *Gramd4*$^{w/w}$ (red) and *Gramd4*$^{sp/sp}$ (blue), and horizontal lines represent means.
(I) Schematic representation of the experimental setup in (J) and (K).
(J) Representative flow cytometry plot for OT-II CD4$^+$ T cell activation (CTV dilution after immunization with OVA$^{328–339}$ peptide in alum) in popliteal LN of *Gramd4*$^{w/w}$ and *Gramd4*$^{sp/sp}$ recipient mice. Graph shows the absolute numbers of OT-II cells in popliteal lymph nodes and the x axis the number of divisions after immunization.
(K) CD69 and CD43 expression of divided OT-II T cells in popliteal LN of *Gramd4*$^{w/w}$ and *Gramd4*$^{sp/sp}$ recipient mice. Each dot represents one mouse, $n = 6$ per group, *Gramd4*$^{w/w}$ (orange) and *Gramd4*$^{sp/sp}$ (green), and horizontal lines represent means (J and K). Student's t test, $^*p < 0.05$, $^{**}p < 0.01$, $^{***}p < 0.001$, $^{****}p < 0.0001$. iLN (inguinal LN).

CellPress
OPEN ACCESS

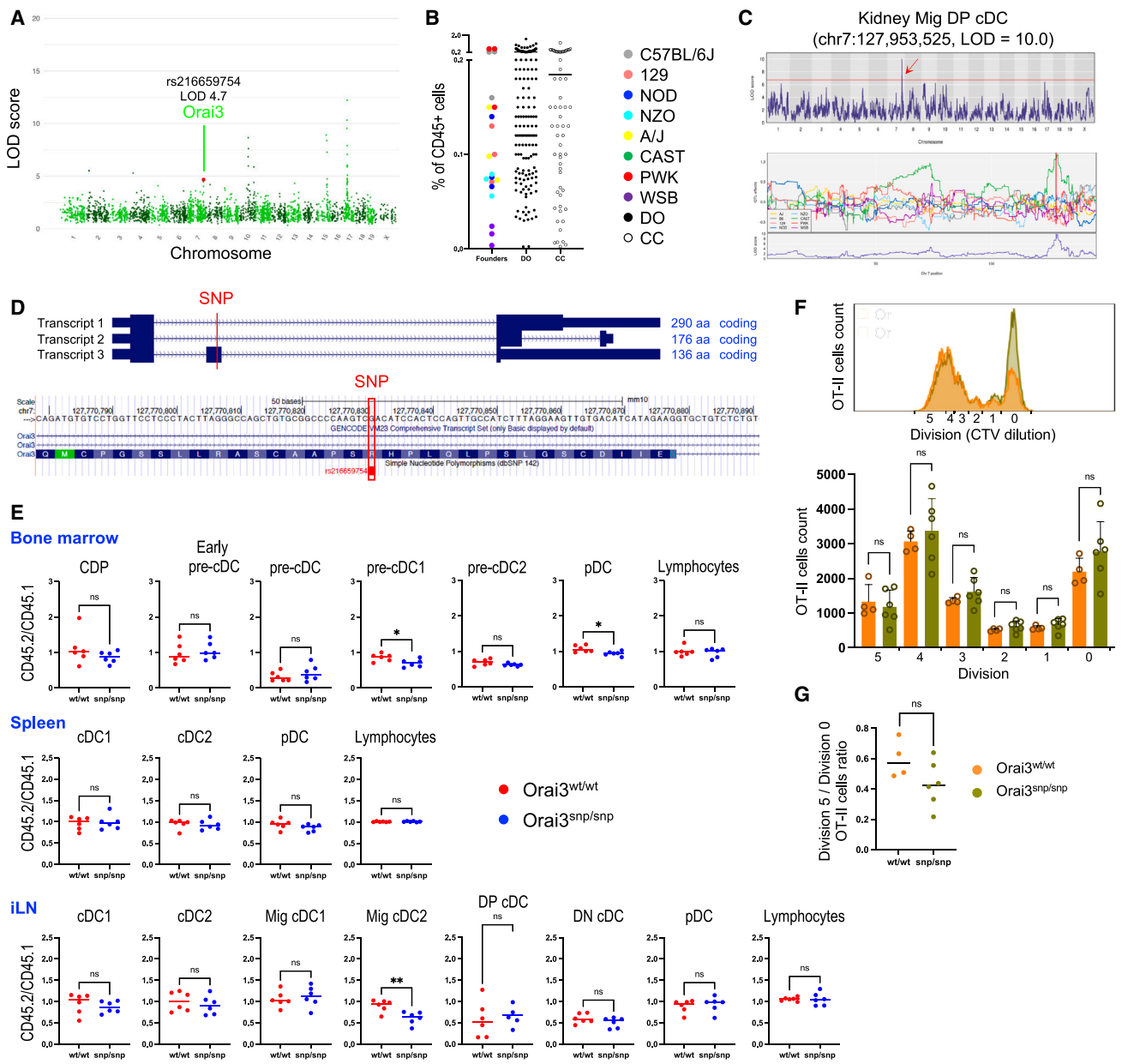


**Figure 6. *Orai3* drives the frequency of migratory cDC2s**

(A) Manhattan plot showing all missense variant SNPs across the 49 phenotypes. For each missense variant, the best *p* value observed among all assessed traits is plotted on a –log10 scale (y axis), according to its genomic coordinates (x axis). *Orai3* missense variant chosen for validation is highlighted in red.

(B) Variation in frequency of kidney Mig DP cDCs in C57BL/6J (gray; $n = 3$), 129 (pink; $n = 3$), NOD (blue; $n = 3$), NZO (cyan; $n = 3$), A/J (yellow; $n = 3$), PWK (red; $n = 3$), WSB (purple; $n = 3$), DO (black; $n = 181$), and CC-RI (open; $n = 59$) mice.

(C) A QTL driving the frequency of kidney Mig DP cDCs found within chromosome 7 (chr7:127,953,525, LOD = 10.0) driven largely by a CAST founder effect.

(D) *Orai3* gene structure and schematic representation of alternative transcript (UCSC Genome Browser). SNP localization is shown in red.

(E) Frequencies of DC progenitors and subsets in mixed BM chimera mice due to differential expression of *Orai3* SNP variant in BM, spleen, and inguinal LN. Chimerism is expressed as the ratio between the number of CD45.2 and CD45.1/CD45.2 cells for each cell population. See schematic representation of the experimental setup in Figures 5F and 5G. Representative of 2 independent experiments; each circle represents one mouse, $n = 6$ per group, $Orai3^{w/w}$ (red) and $Orai3^{snp/snp}$ (blue), and horizontal lines represent means.

(F) Representative flow cytometry plot for OT-II $CD4^+$ T cell activation (CTV dilution after immunization with $OVA^{328–339}$ peptide in alum) in popliteal LN of $Orai3^{w/w}$ and $Orai3^{sp/sp}$ recipient mice. Graph shows the absolute numbers of OT-II cells in popliteal lymph nodes and the x axis the number of divisions after immunization. See schematic representation of the experimental setup in Figure 5I.

(G) Plots show the ratio of fully divided (division 5) to undivided (division 0) OT-II cells in popliteal LN of $Orai3^{w/w}$ and $Orai3^{sp/sp}$ recipient mice. Each dot represents one mouse, $n = 6$ per group, $Orai3^{w/w}$ (orange) and $Orai3^{sp/sp}$ (green), and horizontal lines represent means (F and G). Student's t test, $^*p < 0.05$, $^{**}p < 0.01$, $^{***}p < 0.001$, $^{****}p < 0.0001$. iLN (inguinal LN).

*Orai3* is found within a QTL in chromosome 7 (Chr7: 127,953,525, LOD = 10.0) and was identified in migratory DP cDCs in kidney (Figure 6B). This QTL has a relatively high LOD score (LOD = 10.0) and maps to an interval encompassing known markers such as CD11c and CD11b. Because a CAST allele was the sole allele contributing to phenotypic differences, we focused on private CAST variants (Figure 6C). There are a total of 46 SNPs across CC and DO mice within this QTL, with LOD score ranging from 4.5 to 5.5, which are all private CAST SNPs (Table S4). There are SNPs in 25 genes in this genomic region (*BC017158*, *Tgfb1i1*, *Cox6a2*, *Itgam*, *Itgax*, *Fus*, *Bckdk*, *Stx4a*, *Stx1b*, *Bcl7c*, *Rnf40*, *Rgs10*, *Setd1a*, *Trim72*, *Orai3*, *Prss53*, *Zfp629*, *Zfp668*, *Srcap*, *Ctf2*, *9130023H24Rik*, *Itgad*, and *Prss36*). Of these, there is only one coding SNP, a missense variant in *Orai3* (Figure 6D). *Orai3* is a member of the Orai family (Orai1–3) and a component of the store-operated $Ca^{2+}$ entry channels, which have been shown to play a role in cell proliferation and cell cycle progression.[83] *Orai3* is expressed in all leukocytes. However, the physiological role of *Orai3* in immune cells remains elusive. We used CRISPR-Cas9 to introduce the relevant missense mutation into the genome of C57BL/6J mice ($Orai3^{snp/snp}$) (Figure 6D). To determine whether the $Orai3^{snp/snp}$ variant produces an advantage in DC development, we created 50:50 $Orai3^{snp/snp}$:$Orai3^{w/w}$ BM chimeric mice using CD45.1 or .2 to identify the two donors. Homozygous $Orai3^{snp/snp}$ mice were born at normal Mendelian frequencies. As shown in Figure 6E, we analyzed the DC lineage-specific chimerism and showed a decrease in migratory cDC2 subset frequencies bearing the SNP in iLN. Finally, to determine whether this difference in migratory cDC2 frequencies could modulate T cell responses, we enumerated transferred OT-II cells in the popliteal LNs of $OVA^{328–339}$-immunized $Orai3^{snp/snp}$ and $Orai3^{w/w}$ mice. While OT-II cell recruitment and proliferation in draining LNs is not statistically different between the two types of mice (Figure 6F), the ratio of divided to undivided OT-II cells in $Orai3^{snp/snp}$ mice tends to be lower than in $Orai3^{w/w}$ mice, suggesting a potential disadvantage of OT-II T cell proliferation in the $Orai3^{snp/snp}$ mice (Figure 6G). In conclusion, *Orai3* regulates the number of migratory cDC2s in tissues.

## DISCUSSION

We have examined the genetic control of DC homeostasis in the BM and peripheral tissues in mice. Analysis of DC distribution in multiple tissues in different inbred strains of mice showed that each population of DCs displayed characteristic features. The genetic control of these features was subsequently analyzed using CC and DO mice derived from the original 8 inbred strains. The analysis produced a 1-Mb interval map of the genetic regions that regulate DC numbers. Within those intervals, we identified 104 candidate genes, some of which corresponded to previously identified regulators of DC development. Two of these genes, *Gramd4* that controls DC development in the BM and *Orai3* that regulates cDC2 numbers in tissues, were verified by CRISPR-Cas9 modification of the C57BL/6J mouse genome. The DC phenotype and changes in T cell responses observed in *Gramd4* or *Orai3* mutant mice were modest. This observation is in keeping with the finding that DC homeostasis is a complex trait with a highly polygenic, pleiotropic, and epistatic architecture.

Our approach combined CC and DO mice to enhance the precision of the genetic mapping approach. CC strains, which are syngeneic, can map QTLs to 4- to 6-Mb intervals.[53,63] By combining CC with DO mice, which are more representative of an outbred population, we reduced the QTL intervals to 1 Mb centered on the peak and reduced the number of mice required for the analysis. This general approach increases resolution and facilitates genetic mapping of complex traits.

DCs are found throughout the body in lymphoid and non-lymphoid tissues. Their development begins in the BM, which exports immature cells whose development is completed in the periphery. Genetic regulation of DC development is most evident in the BM as evidenced by genetic intervals with the highest LOD scores. This group of genes is exemplified by *Gramd4*, *Itgb2*, and *Zfat* that contribute to the control of shared aspects of pDC, cDC1, and cDC2 development. In addition to genes that regulate shared aspects of DC development, intervals with high LOD scores are also associated with pDC and cDC1 development in the BM as exemplified by *Kif11* and *Plcg2*. The identification of genes with high LOD scores regulating pDC and cDC1 but not cDC2 development in the BM is consistent with earlier studies showing that *Irf8* and *Batf3* regulate cDC1 and that *Irf8* and *Bcl11a* regulate pDC development in this tissue.[9,74,84–86]

DC development continues after they migrate to lymphoid tissues. In particular, we find genes with high LOD scores associated with cDC2 development in the periphery as exemplified by *Lst1*, *Tnf*, *Ltb*, *Brd2*, and *Unca45a*, which regulate the number of cDC2s in LNs. Thus, whereas the genetic control of pDCs and cDC1s is dominated by genes expressed early in development, genes with high LOD scores control cDC2 numbers in peripheral lymphoid tissues.

DC numbers in non-lymphoid tissues greatly varied among the 8 founder strains. For example, the number of DCs in intestine in 129 mice was 50-fold greater than in PWK mice. In contrast to the lymphoid tissues where a relatively small number of genes with high LOD scores controlled DC numbers, we found that there were a large number of genes with relatively low LOD scores that were associated with non-lymphoid tissue DC number variation.

In conclusion, our data represent a comprehensive analysis of the genetic regulation underlying DC homeostasis. Through the analysis of lymphoid and non-lymphoid tissues, we revealed genetic variants associated with DC abundance and validated two coding genetic variants, i.e., *Gramd4* and *Orai3*. Overall, the data represent a resource for interrogating the mechanisms governing DC homeostasis in tissues.

### Limitations of the study

By using CD8α/CD103 instead of XCR1 to identify cDC1s, we did not distinguish between immediate precursors and fully differentiated cDC1s in the DN cDC compartment. By doing so, we underestimated the numbers of mature cDC1s. Our analysis revealed 101 QTLs linked to DC homeostasis, most of the QTLs being of small effect and fewer QTLs of larger effect. The strongest QTLs are found in lymphoid tissues, which suggests that the

genetic regulation is stronger in these tissues than in non-lymphoid tissues. Because validation of candidate genes requires labor-intensive and costly genetic engineering, we chose to focus on *Gramd4* and *Orai3* that were identified in large-effect QTLs. Although our approach lacks power in accurately mapping non-lymphoid tissue QTLs, genes associated with small-effect QTLs could be tested if additional data such as gene expression or legacy associations are available. Our analysis did not allow us to determine if identification of QTLs in non-lymphoid tissues was challenging because of (1) the sample size, (2) the small influence of these QTLs on the phenotype, or (3) the more complex genetic regulation potentially involving gene interaction in these tissues. Moreover, our study did not allow us to determine if the effects mediated through *Gramd4* and *Orai3* are DC intrinsic or tissue specific. We did not determine the additive effect or epistatic effect of *Gramd4* and *Orai3* on DC homeostasis. Lastly, we co-housed the CC and DO mice in the same facility to minimize the effect of environmental factors on phenotype variation. However, the microbiome could explain some of the observed variation, especially in non-lymphoid tissues such as the intestine.

## STAR★METHODS

Detailed methods are provided in the online version of this paper and include the following:

- KEY RESOURCES TABLE
- RESOURCE AVAILABILITY
  - Lead contact
  - Materials availability
  - Data and code availability
- EXPERIMENTAL MODEL AND SUBJECT DETAILS
  - Mice
- METHOD DETAILS
  - Single cell suspension preparation
  - Flow cytometry antibodies and reagents
  - Flow cytometry analysis
  - Mixed BM chimera
  - T cell activation *in vivo*
  - Immunoblotting
  - Generation of Gramd4$^{sp/sp}$ and Orai3$^{snp/snp}$ mice by CRISPR-Cas9 genome editing
  - Genotyping
- QUANTIFICATION AND STATISTICAL ANALYSIS
  - Power analysis
  - High-resolution QTL mapping analysis
  - UMAP and correlation heatmap
  - Statistical analyses

## SUPPLEMENTAL INFORMATION

Supplemental information can be found online at https://doi.org/10.1016/j.celrep.2024.114296.

## ACKNOWLEDGMENTS

We thank all Nussenzweig Lab members, particularly A. Gazumyan, P. Mendoza, and L. Nogueira. We thank members of the Mucida Lab, B. Reis, A. Bilate, A. Lockhart, and M.C. Campos Canesso for experimental assistance. We also thank the Rockefeller University employees for their continuous assistance. This work was supported by NIH (1R21AI145369) to G.B., NIH (R01GM070683) to G.A.C. and D.M.G., and Stavros Niarchos Foundation to M.C.N. This work was supported in part by the NIH National Center for Research Resources (2UL1RR024143). J.M. is a Branco Weiss Fellow. M.C.N. is an HHMI investigator. This article is subject to HHMI's Open Access to Publications policy.

## AUTHOR CONTRIBUTIONS

Conceptualization, G.B. and M.C.N.; data analysis, G.B., T.Y.O., D.M.G., G.A.C., and M.C.N.; experimental procedures, G.B., J.M., T.E., J.B., and K.-H.Y.; writing—original draft, G.B. and M.C.N.; writing—review & editing, G.B., T.Y.O., G.A.C., and M.C.N.

## DECLARATION OF INTERESTS

The authors declare no competing interests.

Received: December 7, 2023
Revised: April 2, 2024
Accepted: May 14, 2024
Published: May 31, 2024

## REFERENCES

1. Cabeza-Cabrerizo, M., Cardoso, A., Minutti, C.M., Pereira da Costa, M., and Reis e Sousa, C. (2021). Dendritic Cells Revisited. Annu. Rev. Immunol. *39*, 131–166. https://doi.org/10.1146/annurev-immunol-061020-053707.
2. Durai, V., and Murphy, K.M. (2016). Functions of Murine Dendritic Cells. Immunity *45*, 719–736.
3. Merad, M., Sathe, P., Helft, J., Miller, J., and Mortha, A. (2013). The dendritic cell lineage: ontogeny and function of dendritic cells and their subsets in the steady state and the inflamed setting. Annu. Rev. Immunol. *31*, 563–604.
4. Steinman, R.M., Bonifaz, L., Fujii, S.i., Liu, K., Bonnyay, D., Yamazaki, S., Pack, M., Hawiger, D., Iyoda, T., Inaba, K., and Nussenzweig, M.C. (2005). The innate functions of dendritic cells in peripheral lymphoid tissues. Adv. Exp. Med. Biol. *560*, 83–97. https://doi.org/10.1007/0-387-24180-9_12.
5. Banchereau, J., and Steinman, R.M. (1998). Dendritic cells and the control of immunity. Nature *392*, 245–252. https://doi.org/10.1038/32588.
6. Reizis, B. (2019). Plasmacytoid Dendritic Cells: Development, Regulation, and Function. Immunity *50*, 37–50.
7. Bachem, A., Güttler, S., Hartung, E., Ebstein, F., Schaefer, M., Tannert, A., Salama, A., Movassaghi, K., Opitz, C., Mages, H.W., et al. (2010). Superior antigen cross-presentation and XCR1 expression define human CD11c+CD141+ cells as homologues of mouse CD8+ dendritic cells. J. Exp. Med. *207*, 1273–1281.
8. Dorner, B.G., Dorner, M.B., Zhou, X., Opitz, C., Mora, A., Güttler, S., Hutloff, A., Mages, H.W., Ranke, K., Schaefer, M., et al. (2009). Selective expression of the chemokine receptor XCR1 on cross-presenting dendritic cells determines cooperation with CD8+ T cells. Immunity *31*, 823–833. https://doi.org/10.1016/j.immuni.2009.08.027.
9. Hildner, K., Edelson, B.T., Purtha, W.E., Diamond, M., Matsushita, H., Kohyama, M., Calderon, B., Schraml, B.U., Unanue, E.R., Diamond, M.S., et al. (2008). Batf3 deficiency reveals a critical role for CD8alpha+ dendritic cells in cytotoxic T cell immunity. Science *322*, 1097–1100.
10. Williams, J.W., Tjota, M.Y., Clay, B.S., Vander Lugt, B., Bandukwala, H.S., Hrusch, C.L., Decker, D.C., Blaine, K.M., Fixsen, B.R., Singh, H., et al. (2013). Transcription factor IRF4 drives dendritic cells to promote Th2 differentiation. Nat. Commun. *4*, 2990.
11. Gao, Y., Nish, S.A., Jiang, R., Hou, L., Licona-Limón, P., Weinstein, J.S., Zhao, H., and Medzhitov, R. (2013). Control of T helper 2 responses by transcription factor IRF4-dependent dendritic cells. Immunity *39*, 722–732.
12. Persson, E.K., Uronen-Hansson, H., Semmrich, M., Rivollier, A., Hägerbrand, K., Marsal, J., Gudjonsson, S., Håkansson, U., Reizis, B., Kotarsky, K., and Agace, W.W. (2013). IRF4 transcription-factor-dependent

CD103(+)CD11b(+) dendritic cells drive mucosal T helper 17 cell differentiation. Immunity *38*, 958–969. https://doi.org/10.1016/j.immuni.2013.03.009.

13. Schlitzer, A., McGovern, N., Teo, P., Zelante, T., Atarashi, K., Low, D., Ho, A.W.S., See, P., Shin, A., Wasan, P.S., et al. (2013). IRF4 transcription factor-dependent CD11b+ dendritic cells in human and mouse control mucosal IL-17 cytokine responses. Immunity *38*, 970–983.
14. Dudziak, D., Kamphorst, A.O., Heidkamp, G.F., Buchholz, V.R., Trumpfheller, C., Yamazaki, S., Cheong, C., Liu, K., Lee, H.W., Park, C.G., et al. (2007). Differential antigen processing by dendritic cell subsets in vivo. Science *315*, 107–111. https://doi.org/10.1126/science.1136080.
15. Liu, K., and Nussenzweig, M.C. (2010). Origin and development of dendritic cells. Immunol. Rev. *234*, 45–54. https://doi.org/10.1111/j.0105-2896.2009.00879.x.
16. Lee, J., Zhou, Y.J., Ma, W., Zhang, W., Aljoufi, A., Luh, T., Lucero, K., Liang, D., Thomsen, M., Bhagat, G., et al. (2017). Lineage specification of human dendritic cells is marked by IRF8 expression in hematopoietic stem cells and multipotent progenitors. Nat. Immunol. *18*, 877–888.
17. Fogg, D.K., Sibon, C., Miled, C., Jung, S., Aucouturier, P., Littman, D.R., Cumano, A., and Geissmann, F. (2006). A clonogenic bone marrow progenitor specific for macrophages and dendritic cells. Science *311*, 83–87. https://doi.org/10.1126/science.1117729.
18. Naik, S.H., Perié, L., Swart, E., Gerlach, C., van Rooij, N., de Boer, R.J., and Schumacher, T.N. (2013). Diverse and heritable lineage imprinting of early haematopoietic progenitors. Nature *496*, 229–232. https://doi.org/10.1038/nature12013.
19. Lee, J., Breton, G., Oliveira, T.Y.K., Zhou, Y.J., Aljoufi, A., Puhr, S., Cameron, M.J., Sékaly, R.P., Nussenzweig, M.C., and Liu, K. (2015). Restricted dendritic cell and monocyte progenitors in human cord blood and bone marrow. J. Exp. Med. *212*, 385–399.
20. Naik, S.H., Sathe, P., Park, H.Y., Metcalf, D., Proietto, A.I., Dakic, A., Carotta, S., O'Keeffe, M., Bahlo, M., Papenfuss, A., et al. (2007). Development of plasmacytoid and conventional dendritic cell subtypes from single precursor cells derived in vitro and in vivo. Nat. Immunol. *8*, 1217–1226. https://doi.org/10.1038/ni1522.
21. Onai, N., Obata-Onai, A., Schmid, M.A., Ohteki, T., Jarrossay, D., and Manz, M.G. (2007). Identification of clonogenic common Flt3+M-CSFR+ plasmacytoid and conventional dendritic cell progenitors in mouse bone marrow. Nat. Immunol. *8*, 1207–1216. https://doi.org/10.1038/ni1518.
22. Breton, G., Lee, J., Zhou, Y.J., Schreiber, J.J., Keler, T., Puhr, S., Anandasabapathy, N., Schlesinger, S., Caskey, M., Liu, K., and Nussenzweig, M.C. (2015). Circulating precursors of human CD1c+ and CD141+ dendritic cells. J. Exp. Med. *212*, 401–413.
23. Liu, K., Victora, G.D., Schwickert, T.A., Guermonprez, P., Meredith, M.M., Yao, K., Chu, F.F., Randolph, G.J., Rudensky, A.Y., and Nussenzweig, M. (2009). In vivo analysis of dendritic cell development and homeostasis. Science *324*, 392–397.
24. Breton, G., Zheng, S., Valieris, R., Tojal da Silva, I., Satija, R., and Nussenzweig, M.C. (2016). Human dendritic cells (DCs) are derived from distinct circulating precursors that are precommitted to become CD1c+ or CD141+ DCs. J. Exp. Med. *213*, 2861–2870.
25. Schlitzer, A., Sivakamasundari, V., Chen, J., Sumatoh, H.R.B., Schreuder, J., Lum, J., Malleret, B., Zhang, S., Larbi, A., Zolezzi, F., et al. (2015). Identification of cDC1- and cDC2-committed DC progenitors reveals early lineage priming at the common DC progenitor stage in the bone marrow. Nat. Immunol. *16*, 718–728. https://doi.org/10.1038/ni.3200.
26. Ginhoux, F., Liu, K., Helft, J., Bogunovic, M., Greter, M., Hashimoto, D., Price, J., Yin, N., Bromberg, J., Lira, S.A., et al. (2009). The origin and development of nonlymphoid tissue CD103+ DCs. J. Exp. Med. *206*, 3115–3130.
27. Edelson, B.T., Kc, W., Juang, R., Kohyama, M., Benoit, L.A., Klekotka, P.A., Moon, C., Albring, J.C., Ise, W., Michael, D.G., et al. (2010). Peripheral CD103+ dendritic cells form a unified subset developmentally related to CD8alpha+ conventional dendritic cells. J. Exp. Med. *207*, 823–836.
28. Arroyo Hornero, R., and Idoyaga, J. (2023). Plasmacytoid dendritic cells: A dendritic cell in disguise. Mol. Immunol. *159*, 38–45. https://doi.org/10.1016/j.molimm.2023.05.007.
29. Dress, R.J., Dutertre, C.A., Giladi, A., Schlitzer, A., Low, I., Shadan, N.B., Tay, A., Lum, J., Kairi, M.F.B.M., Hwang, Y.Y., et al. (2019). Plasmacytoid dendritic cells develop from Ly6D(+) lymphoid progenitors distinct from the myeloid lineage. Nat. Immunol. *20*, 852–864. https://doi.org/10.1038/s41590-019-0420-3.
30. Feng, J., Pucella, J.N., Jang, G., Alcántara-Hernández, M., Upadhaya, S., Adams, N.M., Khodadadi-Jamayran, A., Lau, C.M., Stoeckius, M., Hao, S., et al. (2022). Clonal lineage tracing reveals shared origin of conventional and plasmacytoid dendritic cells. Immunity *55*, 405–422.e11. https://doi.org/10.1016/j.immuni.2022.01.016.
31. Zhan, Y., Chow, K.V., Soo, P., Xu, Z., Brady, J.L., Lawlor, K.E., Masters, S.L., O'Keeffe, M., Shortman, K., Zhang, J.G., and Lew, A.M. (2016). Plasmacytoid dendritic cells are short-lived: reappraising the influence of migration, genetic factors and activation on estimation of lifespan. Sci. Rep. *6*, 25060.
32. Kamath, A.T., Henri, S., Battye, F., Tough, D.F., and Shortman, K. (2002). Developmental kinetics and lifespan of dendritic cells in mouse lymphoid organs. Blood *100*, 1734–1741.
33. Hou, W.S., and Van Parijs, L. (2004). A Bcl-2-dependent molecular timer regulates the lifespan and immunogenicity of dendritic cells. Nat. Immunol. *5*, 583–589. https://doi.org/10.1038/ni1071.
34. Nopora, A., and Brocker, T. (2002). Bcl-2 controls dendritic cell longevity in vivo. J. Immunol. *169*, 3006–3014. https://doi.org/10.4049/jimmunol.169.6.3006.
35. Liu, K., Waskow, C., Liu, X., Yao, K., Hoh, J., and Nussenzweig, M. (2007). Origin of dendritic cells in peripheral lymphoid organs of mice. Nat. Immunol. *8*, 578–583. https://doi.org/10.1038/ni1462.
36. Waskow, C., Liu, K., Darrasse-Jèze, G., Guermonprez, P., Ginhoux, F., Merad, M., Shengelia, T., Yao, K., and Nussenzweig, M. (2008). The receptor tyrosine kinase Flt3 is required for dendritic cell development in peripheral lymphoid tissues. Nat. Immunol. *9*, 676–683.
37. Kingston, D., Schmid, M.A., Onai, N., Obata-Onai, A., Baumjohann, D., and Manz, M.G. (2009). The concerted action of GM-CSF and Flt3-ligand on in vivo dendritic cell homeostasis. Blood *114*, 835–843. https://doi.org/10.1182/blood-2009-02-206318.
38. Greter, M., Helft, J., Chow, A., Hashimoto, D., Mortha, A., Agudo-Cantero, J., Bogunovic, M., Gautier, E.L., Miller, J., Leboeuf, M., et al. (2012). GM-CSF controls nonlymphoid tissue dendritic cell homeostasis but is dispensable for the differentiation of inflammatory dendritic cells. Immunity *36*, 1031–1046.
39. Worbs, T., Hammerschmidt, S.I., and Förster, R. (2017). Dendritic cell migration in health and disease. Nat. Rev. Immunol. *17*, 30–48. https://doi.org/10.1038/nri.2016.116.
40. Wendland, M., Willenzon, S., Kocks, J., Davalos-Misslitz, A.C., Hammerschmidt, S.I., Schumann, K., Kremmer, E., Sixt, M., Hoffmeyer, A., Pabst, O., and Förster, R. (2011). Lymph node T cell homeostasis relies on steady state homing of dendritic cells. Immunity *35*, 945–957. https://doi.org/10.1016/j.immuni.2011.10.017.
41. Darrasse-Jèze, G., Deroubaix, S., Mouquet, H., Victora, G.D., Eisenreich, T., Yao, K.H., Masilamani, R.F., Dustin, M.L., Rudensky, A., Liu, K., and Nussenzweig, M.C. (2009). Feedback control of regulatory T cell homeostasis by dendritic cells in vivo. J. Exp. Med. *206*, 1853–1862.
42. Chen, M., Wang, Y.H., Wang, Y., Huang, L., Sandoval, H., Liu, Y.J., and Wang, J. (2006). Dendritic cell apoptosis in the maintenance of immune tolerance. Science *311*, 1160–1164. https://doi.org/10.1126/science.1122545.

43. Chen, M., Huang, L., and Wang, J. (2007). Deficiency of Bim in dendritic cells contributes to overactivation of lymphocytes and autoimmunity. Blood *109*, 4360–4367.

44. Stranges, P.B., Watson, J., Cooper, C.J., Choisy-Rossi, C.M., Stonebraker, A.C., Beighton, R.A., Hartig, H., Sundberg, J.P., Servick, S., Kaufmann, G., et al. (2007). Elimination of antigen-presenting cells and autoreactive T cells by Fas contributes to prevention of autoimmunity. Immunity *26*, 629–641.

45. Ohnmacht, C., Pullner, A., King, S.B.S., Drexler, I., Meier, S., Brocker, T., and Voehringer, D. (2009). Constitutive ablation of dendritic cells breaks self-tolerance of CD4 T cells and results in spontaneous fatal autoimmunity. J. Exp. Med. *206*, 549–559.

46. Park, D., Lapteva, N., Seethammagari, M., Slawin, K.M., and Spencer, D.M. (2006). An essential role for Akt1 in dendritic cell function and tumor immunotherapy. Nat. Biotechnol. *24*, 1581–1590. https://doi.org/10.1038/nbt1262.

47. Jung, S., Unutmaz, D., Wong, P., Sano, G.I., De los Santos, K., Sparwasser, T., Wu, S., Vuthoori, S., Ko, K., Zavala, F., et al. (2002). In vivo depletion of CD11c+ dendritic cells abrogates priming of CD8+ T cells by exogenous cell-associated antigens. Immunity *17*, 211–220.

48. Birnberg, T., Bar-On, L., Sapoznikov, A., Caton, M.L., Cervantes-Barragán, L., Makia, D., Krauthgamer, R., Brenner, O., Ludewig, B., Brockschnieder, D., et al. (2008). Lack of conventional dendritic cells is compatible with normal development and T cell homeostasis, but causes myeloid proliferative syndrome. Immunity *29*, 986–997. https://doi.org/10.1016/j.immuni.2008.10.012.

49. Rubelt, F., Bolen, C.R., McGuire, H.M., Vander Heiden, J.A., Gadala-Maria, D., Levin, M., Euskirchen, G.M., Mamedov, M.R., Swan, G.E., Dekker, C.L., et al. (2016). Individual heritable differences result in unique cell lymphocyte receptor repertoires of naïve and antigen-experienced cells. Nat. Commun. *7*, 11112.

50. Hall, M.A., Ahmadi, K.R., Norman, P., Snieder, H., MacGregor, A.J., Vaughan, R.W., Spector, T.D., and Lanchbury, J.S. (2000). Genetic influence on peripheral blood T lymphocyte levels. Genes Immun. *1*, 423–427. https://doi.org/10.1038/sj.gene.6363702.

51. Mangino, M., Roederer, M., Beddall, M.H., Nestle, F.O., and Spector, T.D. (2017). Innate and adaptive immune traits are differentially affected by genetic and environmental factors. Nat. Commun. *8*, 13850.

52. Brodin, P., Jojic, V., Gao, T., Bhattacharya, S., Angel, C.J.L., Furman, D., Shen-Orr, S., Dekker, C.L., Swan, G.E., Butte, A.J., et al. (2015). Variation in the human immune system is largely driven by non-heritable influences. Cell *160*, 37–47.

53. Patin, E., Hasan, M., Bergstedt, J., Rouilly, V., Libri, V., Urrutia, A., Alanio, C., Scepanovic, P., Hammer, C., Jönsson, F., et al. (2018). Natural variation in the parameters of innate immune cells is preferentially driven by genetic factors. Nat. Immunol. *19*, 302–314. https://doi.org/10.1038/s41590-018-0049-7.

54. Scepanovic, P., Alanio, C., Hammer, C., Hodel, F., Bergstedt, J., Patin, E., Thorball, C.W., Chaturvedi, N., Charbit, B., Abel, L., et al. (2018). Human genetic variants and age are the strongest predictors of humoral immune responses to common pathogens and vaccines. Genome Med. *10*, 59.

55. Piasecka, B., Duffy, D., Urrutia, A., Quach, H., Patin, E., Posseme, C., Bergstedt, J., Charbit, B., Rouilly, V., MacPherson, C.R., et al. (2018). Distinctive roles of age, sex, and genetics in shaping transcriptional variation of human immune responses to microbial challenges. Proc. Natl. Acad. Sci. USA *115*, E488–E497.

56. Lu, Y., Biancotto, A., Cheung, F., Remmers, E., Shah, N., McCoy, J.P., and Tsang, J.S. (2016). Systematic Analysis of Cell-to-Cell Expression Variation of T Lymphocytes in a Human Cohort Identifies Aging and Genetic Associations. Immunity *45*, 1162–1175.

57. Orrù, V., Steri, M., Sole, G., Sidore, C., Virdis, F., Dei, M., Lai, S., Zoledziewska, M., Busonero, F., Mulas, A., et al. (2013). Genetic variants regulating immune cell levels in health and disease. Cell *155*, 242–256.

58. Roederer, M., Quaye, L., Mangino, M., Beddall, M.H., Mahnke, Y., Chattopadhyay, P., Tosi, I., Napolitano, L., Terranova Barberio, M., Menni, C., et al. (2015). The genetic architecture of the human immune system: a bioresource for autoimmunity and disease pathogenesis. Cell *161*, 387–403.

59. Churchill, G.A., Airey, D.C., Allayee, H., Angel, J.M., Attie, A.D., Beatty, J., Beavis, W.D., Belknap, J.K., Bennett, B., Berrettini, W., et al. (2004). The Collaborative Cross, a community resource for the genetic analysis of complex traits. Nat. Genet. *36*, 1133–1137. https://doi.org/10.1038/ng1104-1133.

60. Churchill, G.A., Gatti, D.M., Munger, S.C., and Svenson, K.L. (2012). The Diversity Outbred mouse population. Mamm. Genome *23*, 713–718.

61. Collaborative Cross Consortium (2012). The genome architecture of the Collaborative Cross mouse genetic reference population. Genetics *190*, 389–401.

62. Graham, J.B., Swarts, J.L., Mooney, M., Choonoo, G., Jeng, S., Miller, D.R., Ferris, M.T., McWeeney, S., and Lund, J.M. (2017). Extensive Homeostatic T Cell Phenotypic Variation within the Collaborative Cross. Cell Rep. *21*, 2313–2325.

63. Phillippi, J., Xie, Y., Miller, D.R., Bell, T.A., Zhang, Z., Lenarcic, A.B., Aylor, D.L., Krovi, S.H., Threadgill, D.W., de Villena, F.P.M., et al. (2014). Using the emerging Collaborative Cross to probe the immune system. Genes Immun. *15*, 38–46.

64. Ferris, M.T., Aylor, D.L., Bottomly, D., Whitmore, A.C., Aicher, L.D., Bell, T.A., Bradel-Tretheway, B., Bryan, J.T., Buus, R.J., Gralinski, L.E., et al. (2013). Modeling host genetic regulation of influenza pathogenesis in the collaborative cross. PLoS Pathog. *9*, e1003196.

65. Rasmussen, A.L., Okumura, A., Ferris, M.T., Green, R., Feldmann, F., Kelly, S.M., Scott, D.P., Safronetz, D., Haddock, E., LaCasse, R., et al. (2014). Host genetic diversity enables Ebola hemorrhagic fever pathogenesis and resistance. Science *346*, 987–991.

66. Gralinski, L.E., Ferris, M.T., Aylor, D.L., Whitmore, A.C., Green, R., Frieman, M.B., Deming, D., Menachery, V.D., Miller, D.R., Buus, R.J., et al. (2015). Genome Wide Identification of SARS-CoV Susceptibility Loci Using the Collaborative Cross. PLoS Genet. *11*, e1005504.

67. Brinkmeyer-Langford, C.L., Rech, R., Amstalden, K., Kochan, K.J., Hillhouse, A.E., Young, C., Welsh, C.J., and Threadgill, D.W. (2017). Host genetic background influences diverse neurological responses to viral infection in mice. Sci. Rep. *7*, 12194.

68. Morgan, A.P., Fu, C.P., Kao, C.Y., Welsh, C.E., Didion, J.P., Yadgary, L., Hyacinth, L., Ferris, M.T., Bell, T.A., Miller, D.R., et al. (2015). The Mouse Universal Genotyping Array: From Substrains to Subspecies. G3 (Bethesda) *6*, 263–279.

69. Svenson, K.L., Gatti, D.M., Valdar, W., Welsh, C.E., Cheng, R., Chesler, E.J., Palmer, A.A., McMillan, L., and Churchill, G.A. (2012). High-resolution genetic mapping using the Mouse Diversity outbred population. Genetics *190*, 437–447.

70. Broman, K.W., Gatti, D.M., Simecek, P., Furlotte, N.A., Prins, P., Sen, Ś., Yandell, B.S., and Churchill, G.A. (2019). R/qtl2: Software for Mapping Quantitative Trait Loci with High-Dimensional Data and Multiparent Populations. Genetics *211*, 495–502.

71. Millstein, J., and Volfson, D. (2013). Computationally efficient permutation-based confidence interval estimation for tail-area FDR. Front. Genet. *4*, 179.

72. Hadeiba, H., Sato, T., Habtezion, A., Oderup, C., Pan, J., and Butcher, E.C. (2008). CCR9 expression defines tolerogenic plasmacytoid dendritic cells able to suppress acute graft-versus-host disease. Nat. Immunol. *9*, 1253–1260.

73. Wendland, M., Czeloth, N., Mach, N., Malissen, B., Kremmer, E., Pabst, O., and Förster, R. (2007). CCR9 is a homing receptor for plasmacytoid dendritic cells to the small intestine. Proc. Natl. Acad. Sci. USA *104*, 6347–6352.

74. Ippolito, G.C., Dekker, J.D., Wang, Y.H., Lee, B.K., Shaffer, A.L., 3rd, Lin, J., Wall, J.K., Lee, B.S., Staudt, L.M., Liu, Y.J., et al. (2014). Dendritic cell

fate is determined by BCL11A. Proc. Natl. Acad. Sci. USA *111*, E998–E1006.

75. Esterházy, D., Canesso, M.C.C., Mesin, L., Muller, P.A., de Castro, T.B.R., Lockhart, A., ElJalby, M., Faria, A.M.C., and Mucida, D. (2019). Compartmentalized gut lymph node drainage dictates adaptive immune responses. Nature *569*, 126–130.
76. Moreira, T.G., Mangani, D., Cox, L.M., Leibowitz, J., Lobo, E.L.C., Oliveira, M.A., Gauthier, C.D., Nakagaki, B.N., Willocq, V., Song, A., et al. (2021). PD-L1(+) and XCR1(+) dendritic cells are region-specific regulators of gut homeostasis. Nat. Commun. *12*, 4907.
77. Sokol, C.L., Camire, R.B., Jones, M.C., and Luster, A.D. (2018). The Chemokine Receptor CCR8 Promotes the Migration of Dendritic Cells into the Lymph Node Parenchyma to Initiate the Allergic Immune Response. Immunity *49*, 449–463.e6.
78. Stevenson, N.J., Addley, M.R., Ryan, E.J., Boyd, C.R., Carroll, H.P., Paunovic, V., Bursill, C.A., Miller, H.C., Channon, K.M., McClurg, A.E., et al. (2009). CCL11 blocks IL-4 and GM-CSF signaling in hematopoietic cells and hinders dendritic cell differentiation via suppressor of cytokine signaling expression. J. Leukoc. Biol. *85*, 289–297. https://doi.org/10.1189/jlb.0708394.
79. Swiecki, M., Miller, H.L., Sesti-Costa, R., Cella, M., Gilfillan, S., and Colonna, M. (2017). Microbiota induces tonic CCL2 systemic levels that control pDC trafficking in steady state. Mucosal Immunol. *10*, 936–945.
80. Lander, E.S., and Botstein, D. (1989). Mapping mendelian factors underlying quantitative traits using RFLP linkage maps. Genetics *121*, 185–199.
81. John, K., Alla, V., Meier, C., and Pützer, B.M. (2011). GRAMD4 mimics p53 and mediates the apoptotic function of p73 at mitochondria. Cell Death Differ. *18*, 874–886.
82. Merkenschlager, J., Finkin, S., Ramos, V., Kraft, J., Cipolla, M., Nowosad, C.R., Hartweger, H., Zhang, W., Olinares, P.D.B., Gazumyan, A., et al. (2021). Dynamic regulation of T(FH) selection during the germinal centre reaction. Nature *591*, 458–463. https://doi.org/10.1038/s41586-021-03187-x.
83. Clemens, R.A., and Lowell, C.A. (2019). CRAC channel regulation of innate immune cells in health and disease. Cell Calcium *78*, 56–65.
84. Grajales-Reyes, G.E., Iwata, A., Albring, J., Wu, X., Tussiwand, R., Kc, W., Kretzer, N.M., Briseño, C.G., Durai, V., Bagadia, P., et al. (2015). Batf3 maintains autoactivation of Irf8 for commitment of a CD8α(+) conventional DC clonogenic progenitor. Nat. Immunol. *16*, 708–717.
85. Kim, S., Bagadia, P., Anderson, D.A., 3rd, Liu, T.T., Huang, X., Theisen, D.J., O'Connor, K.W., Ohara, R.A., Iwata, A., Murphy, T.L., and Murphy, K.M. (2020). High Amount of Transcription Factor IRF8 Engages AP1-IRF Composite Elements in Enhancers to Direct Type 1 Conventional Dendritic Cell Identity. Immunity *53*, 759–774.e9.
86. Sichien, D., Scott, C.L., Martens, L., Vanderkerken, M., Van Gassen, S., Plantinga, M., Joeris, T., De Prijck, S., Vanhoutte, L., Vanheerswynghels, M., et al. (2016). IRF8 Transcription Factor Controls Survival and Function of Terminally Differentiated Conventional and Plasmacytoid Dendritic Cells, Respectively. Immunity *45*, 626–640. https://doi.org/10.1016/j.immuni.2016.08.013.
87. Amend, S.R., Valkenburg, K.C., and Pienta, K.J. (2016). Murine Hind Limb Long Bone Dissection and Bone Marrow Isolation. J. Vis. Exp. Published online April 14. https://doi.org/10.3791/53936.
88. Miura, H., Quadros, R.M., Gurumurthy, C.B., and Ohtsuka, M. (2018). Easi-CRISPR for creating knock-in and conditional knockout mouse models using long ssDNA donors. Nat. Protoc. *13*, 195–215.
89. Gatti, D.M., Svenson, K.L., Shabalin, A., Wu, L.Y., Valdar, W., Simecek, P., Goodwin, N., Cheng, R., Pomp, D., Palmer, A., et al. (2014). Quantitative trait locus mapping methods for diversity outbred mice. G3 (Bethesda) *4*, 1623–1633.
90. Keele, G.R., Crouse, W.L., Kelada, S.N.P., and Valdar, W. (2019). Determinants of QTL Mapping Power in the Realized Collaborative Cross. G3 (Bethesda) *9*, 1707–1727.
91. Sen, S., and Churchill, G.A. (2001). A statistical framework for quantitative trait mapping. Genetics *159*, 371–387.
92. Manichaikul, A., Dupuis, J., Sen, S., and Broman, K.W. (2006). Poor performance of bootstrap confidence intervals for the location of a quantitative trait locus. Genetics *174*, 481–489.

## STAR★METHODS

### KEY RESOURCES TABLE

| REAGENT or RESOURCE | SOURCE | IDENTIFIER |
|---|---|---|
| Antibodies | | |
| FITC Mouse Anti-Mouse I-A[d] _ Clone AMS-32.1 | BD Biosciences | Cat No. 553547; RRID: AB_394914 |
| Alexa Fluor 488 anti-mouse I-A/I-E Antibody _ Clone M5/114.15.2 | Biolegend | Cat No. 107616; RRID: AB_493523 |
| PE anti-mouse DC Marker (33D1) Antibody _ Clone 33D1 | Biolegend | Cat No. 124905; RRID: AB_1186128 |
| PE anti-mouse CD135 Antibody _ Clone A2F10 | Biolegend | Cat No. 135306; RRID: AB_1877217 |
| PE/Dazzle 594 anti-mouse CD103 Antibody _ Clone 2E7 | Biolegend | Cat No. 121430; RRID: AB_2566493 |
| PerCP/Cy5.5 anti-mouse CD317 (BST2, PDCA-1) Antibody | Biolegend | Cat No. 127022; RRID: AB_2566647 |
| PE/Cy7 anti-mouse CD45 Antibody _ Clone 30-F11 | Biolegend | Cat No. 103114; RRID: AB_312979 |
| PE-Cy7 Mouse Anti-Mouse CD45.1 _ Clone A20 | BD Biosciences | Cat No. 560578; RRID: AB_1727488 |
| PE-Cy7 Mouse Anti-Mouse CD45.2 _ Clone 104 | BD Biosciences | Cat No. 560696; RRID: AB_1727494 |
| Brilliant Violet 421 anti-mouse Ly-6C Antibody _ Clone HK1.4 | Biolegend | Cat No. 128032; RRID: AB_2562178 |
| BV510 Rat Anti-Mouse CD11b _ Clone M1/70 | BD Biosciences | Cat No. 562950; RRID: AB_2737913 |
| BV510 Rat Anti-Mouse CD172a _ Clone P84 | BD Biosciences | Cat No. 740159; RRID: AB_2739912 |
| BV605 Rat Anti-Mouse CD117 _ Clone 2B8 | BD Biosciences | Cat No. 563146; RRID: AB_2738028 |
| BV605 Rat Anti-Mouse F4/80-Like Receptor _ Clone 6F12 | BD Biosciences | Cat No. 744337; RRID: AB_2742164 |
| Brilliant Violet 605 anti-mouse F4/80 Antibody _ Clone BM8 | Biolegend | Cat No. 123133; RRID: AB_2562305 |
| BUV805 Rat Anti-Mouse CD4_Clone RM4-5 | BD Biosciences | Cat No. 741912; RRID: AB_2871226 |
| BV711 Rat Anti-Mouse Siglec-F _ Clone E50-2440 | BD Biosciences | Cat No. 740764; RRID: AB_2740427 |
| APC anti-mouse Siglec H Antibody _ Clone 551 | Biolegend | Cat No. 129612; RRID: AB_10641134 |
| APC anti-mouse CD64 (FcγRI) Antibody _ Clone X54-5/7.1 | Biolegend | Cat No. 139306; RRID: AB_11219391 |
| Alexa Fluor 700 Rat Anti-Mouse Ly-6G _ Clone 1A8 | BD Biosciences | Cat No. 561236; RRID: AB_10611860 |
| Alexa Fluor 700 anti-mouse CX3CR1 Antibody _ Clone SA011F11 | Biolegend | Cat No. 149036; RRID: AB_2629606 |
| APC/Cy7 anti-mouse CD115 (CSF-1R) Antibody _ Clone AFS98 | Biolegend | Cat No. 135532; RRID: AB_2632740 |
| CD11c Monoclonal Antibody PE-Cyanine5.5 _ Clone N418 | eBioscience | Cat No. 35-0114-82; RRID: AB_469709 |
| BV786 Rat Anti-Mouse CD19 _ Clone 1D3 | BD Biosciences | Cat No. 563333; RRID: AB_2738141 |
| Brilliant Violet 785 anti-mouse/human CD45R/B220 Antibody _ Clone RA3-6B2 | Biolegend | Cat No. 103246; RRID: AB_2563256 |
| Brilliant Violet 785 anti-mouse NK-1.1 Antibody _ Clone PK136 | Biolegend | Cat No. 108749; RRID: AB_2564304 |
| Brilliant Violet 785 anti-mouse CD3ε Antibody _ Clone 145-2C11 | Biolegend | Cat No. 100355; RRID: AB_2565969 |
| BUV395 Rat Anti-Mouse CD8a _ Clone 53-6.7 | BD Biosciences | Cat No. 563786; RRID: AB_2732919 |
| BUV496 Mouse Anti-Mouse CD45.2 _ Clone 104 | BD Biosciences | Cat No. 741092; RRID: AB_2870691 |
| BUV563 Rat Anti-Mouse CD317 (BST2) _ Clone 927 | BD Biosciences | Cat No. 749275; RRID: AB_2873650 |
| LIVE/DEAD Fixable Blue Dead Cell Stain Kit, for UV excitation | Invitrogen | Cat No. L34962 |
| OneComp eBeads™ Compensation Beads | Invitrogen | Cat No. 01-1111-42 |
| Gramd4 antibody _ Clone C-8 | Santa-Cruz | Cat No. sc-515128 |
| FITC Hamster Anti-Mouse CD69 _Clone H1.2F3 | Biolegend | Cat No. 104506 RRID: AB_313109 |
| PE Rat Anti-Mouse CD43 _ Clone 553271 | BD Biosciences | Cat No. 553271 RRID: AB_394748 |
| CellTrace Violet Cell Proliferation Kit | ThermoFisher Scientific | Cat No. C34557 |
| Chemicals, peptides, and recombinant proteins | | |
| Collagenase D | Roche | Cat No. 11088882001 |
| DNase I | Roche | Cat No. 10104159001 |
| RBC lysis buffer | Roche | Cat No. 11814389001 |

(*Continued on next page*)

| Continued | | |
|---|---|---|
| REAGENT or RESOURCE | SOURCE | IDENTIFIER |
| NP-OVA$^{328-339}$ | This paper | N/A |
| Critical commercial assays | | N/A |
| DNeasy Blood and Tissue Kit | Qiagen | Cat No. 69504 |
| Mouse Universal Genotyping Array (GigaMUGA, 143,259 markers) | Neogen | Cat No. 550 |
| MagniSort™ Mouse CD4 T cell Enrichment Kit | Invitrogen | Cat No. 8804-6821-74 |
| Experimental models: Organisms/strains | | |
| C57BL/6J inbred strain | The Jackson Laboratory | Cat No. 000664; RRID: IMSR_JAX:000664 |
| A/J inbred mice | The Jackson Laboratory | Cat No. 000646; RRID: IMSR_JAX:000646 |
| 129S1/SvlmJ inbred mice | The Jackson Laboratory | Cat No. 002448; RRID: IMSR_JAX:002448 |
| NOD/ShiLtJ inbred mice | The Jackson Laboratory | Cat No. 001976; RRID: IMSR_JAX:001976 |
| NZO/HlLtJ inbred mice | The Jackson Laboratory | Cat No. 002105; RRID: IMSR_JAX:002105 |
| CAST/EiJ inbred mice | The Jackson Laboratory | Cat No. 000928; RRID: IMSR_JAX:000928 |
| PWK/PhJ inbred mice | The Jackson Laboratory | Cat No. 003715; RRID: IMSR_JAX:003715 |
| WSB/EiJ inbred mice | The Jackson Laboratory | Cat No. 001145; RRID: IMSR_JAX:001145 |
| J:DO outbred mice | The Jackson Laboratory | Cat No. 009376; RRID: IMSR_JAX:009376 |
| B6.SJL congenic mice | The Jackson Laboratory | Cat No. 002014; RRID: IMSR_JAX:002014 |
| The Collaborative Cross (CC) recombinant inbred mice | UNC Systems Genetics Core Facility - University of North Carolina at Chapel Hill | N/A |
| OT-II mice | The Jackson Laboratory | Cat No. 004194; RRID: IMSR_JAX:004194 |
| Oligonucleotides | | |
| sgRNA Gramd4: CCAGAAGGTGTGTGCCTGCCCGA | IDT | N/A |
| sgRNA Orai3: CTACTTAGGGCCAGCTGTGCGG | IDT | N/A |
| Primer Gramd4 F1: 5′ CCTCATGGGACCCTTTACC 3′ | IDT | N/A |
| Primer Gramd4 R1: 5′ GGGTTTGATTCCCGGCAGTGTA | IDT | N/A |
| Primer Orai3 F1 5′ CTATATCAACCAGATCGGGGAAGG 3′ | IDT | N/A |
| Primer Orai3 R1 5′ AAGGGTACATTATGAAGGGTGCC 3′ | IDT | N/A |
| Software and algorithms | | |
| DOQTL R package | N/A | https://rdrr.io/bioc/DOQTL/ |
| SPARCC R package | N/A | https://github.com/MPBA/r-sparcc |
| GraphPad Prism | GraphPad | N/A |
| FlowJo | BD Pharmingen | N/A |
| R/QLT2 package | N/A | https://kbroman.org/qtl2/ |
| R/uwot package | N/A | https://github.com/jlmelville/uwot |
| R/stats base package | N/A | https://www.r-project.org |
| ggplot2 | N/A | https://ggplot2.tidyverse.org |
| in-house QTL Viewer written in R Shiny | In this paper | https://zenodo.org/doi/10.5281/zenodo.11127562 |
| Other | | |
| BD FACSymphony A5 Cell Analyzer | BD Biosciences | N/A |

## RESOURCE AVAILABILITY

### Lead contact

Further information and requests for resources and reagents should be directed to and will be fulfilled by the lead contact, Michel C. Nussenzweig (nussen@rockefeller.edu).

### Materials availability

Mouse lines generated in this study are available from the lead contact with a completed Material Transfer Agreement.

### Data and code availability

- All processed data and results can be downloaded and interactively analyzed using the docker image of our QTLViewer webtool (https://hub.docker.com/r/stratust/qtlviewer).
- The source code for the webtool is available at https://zenodo.org/doi/10.5281/zenodo.11127562.
- Any additional information required to reanalyze the data reported in this work paper is available from the lead contact upon request.

## EXPERIMENTAL MODEL AND SUBJECT DETAILS

### Mice

All mice used in this study were housed at The Rockefeller University Comparative for Biosciences Center. All experimental procedures were approved by The Rockefeller University's Institutional Animal Care and Use Committee (IACUC protocol number 19065). We purchased founder mice - C57BL/6J, A/J, 129S1/SvImJ, NOD/ShiLtJ, NZO/HlLtJ, CAST/EiJ, PWK/PhJ, and WSB/EiJ - from The Jackson Laboratory. A total of 189 J:DO females (JAX stock number 009376, outbreeding generations G25 and G26) were purchased from The Jackson Laboratory.[69] 61 CC-RI mouse lines were obtained from the Systems Genetics Core Facility at the University of North Carolina, Chapel Hill (UNC) (Table S6).[59] These 3 stocks of mice were co-housed for 3 weeks prior phenotype screening. We purchased C57BL/6J (CD45.2) and B6.SJL (CD45.1) mice from The Jackson Laboratory and bred C57BL/6J x B6.SJL F1 (CD45.2 x CD45.1) mice. We purchased OT-II (C57BL/6J) mice from The Jackson Laboratory and bred OT-II (CD45.2) x B6.SJL (CD45.1) mice to generate CD45.1 OT-II mice.

## METHOD DETAILS

### Single cell suspension preparation

Spleens and inguinal LN were cut into small pieces and were digested for 30 min at 37°C in a Hanks' balanced salt solution (HBSS) (Gibco) solution containing 400 U/ml Collagenase D (Roche) and 50 μg/mL DNase I (Roche). The cell suspension was then passed through a 70-μm cell strainer. Red blood cells (RBC) were lysed by incubating with RBC lysis buffer (Gibco) for 2 min at room temperature. After washing, cells were then resuspended in 2% (v/v) FBS in PBS and kept at 4°C for subsequent analysis. For BM isolation, femurs and tibias were obtained and the epiphyses of the bones cut off. Bones were then centrifuged to spin out the marrow out of the bones.[87] After RBC lysis, BM is resuspended in 2% (v/v) FBS in PBS and filtered through a 70-μm cell strainer. For lung, liver and kidney cell isolation, tissues were cut into small pieces and then digested for 45 min at 37°C in an HBSS containing 400 U/ml Collagenase D and 50 μg/mL DNase I. Next, the digested tissues were transferred through a 70-μm nylon mesh and mononuclear cells were isolated by gradient centrifugation (underlayer 35% and top layer 70% containing cells) using Percoll (BD Pharmingen). After washing, cells are resuspended in 2% (v/v) FBS in PBS. Small intestine lamina propria mononuclear cells were isolated as previously described.[75] Briefly, small intestines were separated from mesentery and Peyer's Patches, and feces were removed. Small intestines were then washed twice in PBS and 1μM dithiothreitol (DTT) followed by two incubations to remove the epithelium in HBSS, 2% FCS and 30 mM EDTA with vigorous shaking between the two incubations. Tissues were then finely chopped and digested in HBSS 2% FCS containing 2 mg/mL Collagenase 8 (Gibco) and 200 μg/mL DNase I for 45 min at 37°C. Mononuclear cells were isolated by centrifugation in a discontinuous Percoll gradient (40%/80%). Cells were isolated from the interphase, washed, and kept at 4°C for subsequent analysis in PBS 2% FCS. The gut draining LNs were dissected into HBSS supplemented with Mg2+ and Ca2+, finely chopped and incubated in HBSS solution containing 400 U/ml collagenase D for 25 min at 37°C. Tissue dissociation was completed using 18-G syringes and samples were then filtered through 70-μm cell strainers. Erythrocytes were lysed by incubation in RBC lysis buffer for 2 min at room temperature. Cells were resuspended in 2% (v/v) FBS in PBS for downstream flow cytometry.

### Flow cytometry antibodies and reagents

Single cell suspensions were surface stained for 30 min in the dark at 4°C with viability reagent (BD Horizon Fixable Viability Stain, BD Biosciences, San Diego, CA, USA) and a 17-color cocktail of monoclonal antibodies (mAbs) containing surface antibodies against I-A/I-E (Clone M5/114.15.2), I-Ad (clone AMS-32.1), DCIR2 (Clone 33D1), CD103 (Clone 2E7), BTS2 (Clone 927), CD45.1 (Clone A20), CD45.2 (Clone 104), CD45 (clone 30-F11), Ly-6C (Clone HK1.4), CD11b (Clone M1/70), F4/80 (Clone BM8), CD64 (Clone X54-5/7.1), Ly-6G (Clone 1A8), CD11c (Clone N418), Siglec F (Clone E50-2440), CD8a (Clone 53-6.7), CD4 (Clone RM4-5), CD3ε (Clone 145-2C11), CD19 (Clone 1D3), B220 (Clone RA3-6B2), NK-1.1 (Clone PK136), CD135 (Clone A2F10), CD172a (Clone P84), CD117 (Clone 2B8), Siglec H (Clone 551), CX3CR1 (Clone SA011F11), CD69 (Clone H1.2F3) and CD43 (Clone S7). After labeling, cells were washed and fixed in PBS containing 2% paraformaldehyde and stored at 4°C prior to flow cytometry acquisition within 24 h. All events -approximately 1,200,000 to 3,000,000 events per sample-were collected on a BD LSR II Flow Cytometer or a BD FACSymphonyA5 Cell Analyzer (BD Biosciences, San Diego, CA, USA). Cells were gated for further analysis, as described in Figure S1, using Flowjo Software Version 9.9.6 (BD, USA).

### Flow cytometry analysis

To identify DC progenitors and subsets, we used multiparametric flow cytometry (see gating strategy in Figure S1B). As shown in Figure S4A, we observed that three canonical markers i.e., CD45, MHCII and Ly6C, were not observable for some of the three wild-derived strains probably due to reagents being largely developed for laboratory strains. Notably, some CC and DO mice have the wild-derived mice *Cd45*, *MhcII* and/or *Ly6c* alleles. This will affect CD45, MHCII and Ly6C staining for the CC lines which are homozygote but not for the DO mice which are mainly heterozygote. For Ly6C, we considered in the analysis only the mice that were stained by the full set of phenotypic markers i.e., we removed the progenitors but not pDC in BM samples of CAST and PWK homozygote mice ($n$ = 33). For CD45, we kept in the analysis all tissues but removed kidney samples of CAST homozygote mice ($n$ = 10) (Figure S4B). Finally we overcomed the lack of staining for MHCII in PWK and WSB homozygote mice by lowering the gates as shown in Figure S4C.

### Mixed BM chimera

Mixed BM chimeras were performed using 6–8 weeks old, age-matched female mice. Donor BM cells were extracted from the long bones of C57BL/6J mice (CD45.2; wild type or edited) and C57BL/6J x B6.SJL F1 (CD45.1/CD45.2) mice. An equal mix of 5x $10^6$ total cells from CD45.2 and CD45.1/CD45.2 marrow were injected retro-orbitally into lethally irradiated (two radiation doses of 5.5 Gy, 3 h apart) B6.SJL (CD45.1) recipient mice. At week 6 post transfer, organs are harvested, and cells are prepared as described above. Chimerism is expressed as the ratio between the number of CD45.2 and CD45.1/CD45.2) cells.

### T cell activation *in vivo*

OT-II $CD4^+$ T cells (CD45.1) were enriched from spleens using immunomagnetic negative selection (Invitrogen) and labeled with CTV. For adoptive transfer experiments 1x$10^6$ OT-II, CTV labeled cells were injected into recipient mice (CD45.2) by intravenous injection. For NP-$OVA^{328–339}$ hapten-peptide immunizations, recipient mice received 20ul of a 50 μM of hapten-peptide precipitated in alum (adjuvant was used to provide the necessary stimulus to the immune system to allow $CD4^+$ T cell responses) via footpad injection as previously published.[82] The quality of the T cell response was assessed at day 3 in popliteal lymph nodes by enumerating CD45.1+ $CD4^+$ OT-II cells by flow cytometry. The NP-$OVA^{328–339}$ hapten peptide was synthesized in house as previously described.[82]

### Immunoblotting

Splenocytes from both CRISPR-Cas9-edited and unedited Gramd4 mice were prepared as indicated above. Cell pellets were then homogeneized in ice-cold lysing buffer (50 mM Tris HCl, pH 7.7, 150 mM NaCl, 1% NP-40, 1 mM EDTA, 1 mM EGTA, 0.1% DOC, 10% glycerol buffer supplemented with 1 mM PMSF and protease inhibitors) followed by sonication for 10 min. Following incubation on ice for 10 min, samples were centrifuged for 10 min at 14,000 rpm at 4°C. 10 μg, 3.3 μg and 1.1 μg of total protein were resolved on a 4–12% NuPage gel (Invitrogen) and transferred onto Immobilon-P membranes (Millipore). After being blocked, the western blot membrane was subsequently incubated with anti-Gramd4 antibody (Clone C-8, Santa-Cruz).

### Generation of $Gramd4^{sp/sp}$ and $Orai3^{snp/snp}$ mice by CRISPR-Cas9 genome editing

$Gramd4^{sp/sp}$ and $Orai3^{snp/snp}$ mice were generated by CRISPR-Cas 9 genome editing using the Easi-CRISPR protocol[88] to introduce a splice (rs235532740 T|G) and missense (rs216659754 G|A) point mutation for *Gramd4* and *Orai3* respectively. Briefly, fertilized C57BL/6J zygotes at the one-cell stage were cytoplasmically injected with Cas9 protein, sgRNA targeting *Gramd4* (CCAGAAGGTGT GTGCCTGCCCGA) or *Orai3* (CTACTTAGGGCCAGCTGTGCGG) and the corresponding repair ssDNA template. Injected embryos were implanted into pseudo-pregnant foster Swiss animals and mutant offspring were selected by specific PCR genotyping and Sanger DNA sequencing (see below). Mutants were backcrossed to C57BL/6J animals for at least 5 generations. sgRNA and Cas9 protein were purchased from Integrated DNA Technologies (Integrated DNA Technologies). Guides with a MIT score higher than 89 were picked on UCSC Genome Browser. Animals were kept in our facility under The Rockefeller University IACUC protocol.

### Genotyping

CRISPR edited offspring were genotyped from lysed tail DNA samples (QuickExtract DNA Extraction Solution – LGC Biosearch Technologies) by PCR (Platinium Taq DNA Polymerase High Fidelity – Invitrogen) using the primer pair Gramd4 F1: 5′ CCTCATGGGACCC TTTACC 3′, Gramd4 R1: 5′ GGGTTTGATTCCCGGCAGTGTA 3′ and Orai3 F1 5′ CTATATCAACCAGATCGGGGAAGG 3′, Orai3 R1 5′ AAGGGTACATTATGAAGGGTGCC 3′ for 45 cycles (15 s at 94°C, 30 s at 60°C, 1 min at 72°C) to generate a band of 800 bp for *Gramd4* and 600 bp for *Orai3*. PCR products were sequenced by Sanger sequencing.

## QUANTIFICATION AND STATISTICAL ANALYSIS

### Power analysis

Power analysis for the DO mice were done with the freely available DOQTL R package. With a sample size of 189 DO mice, we can detect QTL that explain >20% of the phenotypic variance with 90% power.[89] Importantly this power simulation model was generated in 2014 using the generation G8 of DO animals. As allele frequencies and recombination density are increasing with the number of

generations, 189 DO from G25 and G26 allow to detect loci that account for $\leq$ 20% of trait variance. Sample size and power analysis in CC mice were done with the SPARCC R package. If we screen 61 strains with one observation per strain, a locus with large effect (>20%) has about 5% power.[90] There is no simulation model combining the CC and DO mice.

## High-resolution QTL mapping analysis

### Phenotyping

Tissues from CC and DO mice were processed in batches of ~10 animals each at ages ranging from 8 to 10 weeks. Tissues from each animal were collected and processed immediately after euthanasia. DC frequencies were measured the same day by flow cytometry and calculated as percentages of $CD45^+$ mononuclear cells.

### Genotyping and haplotype reconstructions

Whole genomic DNA was isolated from tail tissue using QIAGEN DNeasy Blood and Tissue Kit per the manufacturer's instructions (QIAGEN, Valencia, CA). CC and DO mice were genotyped using the Mouse Universal Genotyping Array (GigaMUGA, 143,259 markers) (Neogen, Lincoln, NE). Identified genotypes were converted to founder strain–haplotype reconstructions using the R/QLT2 package.

### Interval estimates of QTL location

We performed QTL mapping using the R/QLT2 package for identifying SNP effects based on haplotype.[70] Briefly, R/QLT2 performs QTL genome scans through a regression of the phenotype on genotype probabilities for each of the eight founder strains. A rank *Z* score transformed relative abundances were mapped using a linear mixed model in R-package. A random-effect term is included in the model to account for kinship among animals. A LOD score for each marker is calculated from the likelihood ratio comparing the regression model described above to a regression model without the founder genotype probabilities. QTL intervals were defined by the 95% Bayesian credible interval, calculated by normalizing the area under the QTL curve.[91] We kept only the drop.lod = 1.5 LOD support interval around significant peaks (above lod threshold) at each chromosome for each trait.[92]

### Significance thresholds

The statistical significance of LOD scores is determined via an FDR based permutation approach.[71] Briefly, we calculated FDR for each phenotype separately by shuffling 1,000 times the mice ancestry in the locus and calculating the strength of the association. We used permutation-derived *p*-values and perform an FDR adjustment. An FDR of 5% and less (95th percentile; LOD >8.19), an FDR of 20% and less (85th percentile; LOD >7.47) or an FDR of 40% (62nd percentile; LOD >6.67) was used to select significant associations.

### QTL effect

The formula for converting a LOD to % variance is 100 * (1.0 - exp(-lod * (2 * log(10))/n)) where n is the number of mice.

### SNP associations

The genome-wide SNP association analysis was conducted using the 'scan1snps()' function in R/QLT2. This analysis was performed on a database prepared with the mouse genome build 38 (mm10), which included comprehensive data on all SNPs, along with their respective genotypes across the eight founder strains for both CC and DO populations. We reduced the QTL intervals to 1 Mb centered on the peak to calculate the local LOD score and considered only SNPs that achieve a LOD threshold of 1.5 or less below the top LOD score.[80]

### Rational for combined analysis of CC and DO mice

In our initial QTL mapping efforts, separate analyses for the CC and DO populations revealed a markedly higher number of significant QTL peaks within the DO population, with minimal contributions from the CC population. This disparity led us to a strategic decision to explicitly include the CC data as if it represented a 'first generation' of the DO population. This conceptualization stems from the recognition that the CC lines, despite their inbred nature, encapsulate a broad spectrum of genetic diversity that is foundational to the genetically diverse DO mice.

Particularly, the QTL peaks associated with our candidate genes for validation, namely *Orai3* and *Gramd4*, were predominantly identified within the DO population (Figure S5). The explicit inclusion of CC data, treating these inbred lines as an initial generation within the DO analysis framework, was instrumental in amplifying the signal strength of these QTL peaks. This approach was predicated on the premise that the genetic diversity inherent in the CC lines could significantly enhance the sensitivity and resolution of our QTL mapping. This provided a more nuanced understanding of the genetic architecture influencing the phenotypes under study.

## UMAP and correlation heatmap

We used rank *Z* score transformed phenotypic data and the Euclidean metric to generate a UMAP via the 'umap()' function from the R/uwot package. We calculated pairwise Pearson correlations using the 'cor()' function from the R/stats base package. The correlation heatmap triangle was visualized using ggplot2, and we developed a custom geom to produce diamond-shaped squares.

## Statistical analyses

Statistical analyses were performed using ordinary Student's t-test, as indicated in the figure legends. $^*p < 0.05$, $^{**}p < 0.01$, $^{***}p < 0.001$, $^{****}p < 0.0001$. GraphPad Prism v.10 was used for graphs and statistical analysis.